Passive Acoustic Detection of North Atlantic Right Whales in the Cabot Strait: Ambient Noise Analysis and Detection Range Modelling

Jinshan Xu, Hilary B. Moors-Murphy, and Angelia S.M. Vanderlaan

Fisheries and Oceans Canada
Bedford Institute of Oceanography
Dartmouth, NS
B2Y 4A2

2025

Canadian Technical Report of
Fisheries and Aquatic Sciences 3741

Fisheries and Oceans Canada | Pêches et Océans Canada

Canada

Canadian Technical Report of Fisheries and Aquatic Sciences

Technical reports contain scientific and technical information that contributes to existing knowledge but which is not normally appropriate for primary literature. Technical reports are directed primarily toward a worldwide audience and have an international distribution. No restriction is placed on subject matter and the series reflects the broad interests and policies of Fisheries and Oceans Canada, namely, fisheries and aquatic sciences.

Technical reports may be cited as full publications. The correct citation appears above the abstract of each report. Each report is abstracted in the data base *Aquatic Sciences and Fisheries Abstracts*.

Technical reports are produced regionally but are numbered nationally. Requests for individual reports will be filled by the issuing establishment listed on the front cover and title page.

Numbers 1-456 in this series were issued as Technical Reports of the Fisheries Research Board of Canada. Numbers 457-714 were issued as Department of the Environment, Fisheries and Marine Service, Research and Development Directorate Technical Reports. Numbers 715-924 were issued as Department of Fisheries and Environment, Fisheries and Marine Service Technical Reports. The current series name was changed with report number 925.

Rapport technique canadien des sciences halieutiques et aquatiques

Les rapports techniques contiennent des renseignements scientifiques et techniques qui constituent une contribution aux connaissances actuelles, mais qui ne sont pas normalement appropriés pour la publication dans un journal scientifique. Les rapports techniques sont destinés essentiellement à un public international et ils sont distribués à cet échelon. II n'y a aucune restriction quant au sujet; de fait, la série reflète la vaste gamme des intérêts et des politiques de Pêches et Océans Canada, c'est-à-dire les sciences halieutiques et aquatiques.

Les rapports techniques peuvent être cités comme des publications à part entière. Le titre exact figure au-dessus du résumé de chaque rapport. Les rapports techniques sont résumés dans la base de données *Résumés des sciences aquatiques et halieutiques.*

Les rapports techniques sont produits à l'échelon régional, mais numérotés à l'échelon national. Les demandes de rapports seront satisfaites par l'établissement auteur dont le nom figure sur la couverture et la page du titre.

Les numéros 1 à 456 de cette série ont été publiés à titre de Rapports techniques de l'Office des recherches sur les pêcheries du Canada. Les numéros 457 à 714 sont parus à titre de Rapports techniques de la Direction générale de la recherche et du développement, Service des pêches et de la mer, ministère de l'Environnement. Les numéros 715 à 924 ont été publiés à titre de Rapports techniques du Service des pêches et de la mer, ministère des Pêches et de l'Environnement. Le nom actuel de la série a été établi lors de la parution du numéro 925.

Canadian Technical Report of
Fisheries and Aquatic Sciences 3741

2025

PASSIVE ACOUSTIC DETECTION OF NORTH ATLANTIC RIGHT WHALES IN THE CABOT STRAIT: AMBIENT NOISE ANALYSIS AND DETECTION RANGE MODELLING

by

Jinshan Xu[1], Hilary B. Moors-Murphy[1], and Angelia S.M. Vanderlaan[1]

[1] Fisheries and Oceans Canada
Bedford Institute of Oceanography
Dartmouth, NS
B2Y 4A2

Cat. No. Fs97-6/3741E-PDF ISBN 978-0-660-79987-2 ISSN 1488-5379
https://doi.org/10.60825/r9a8-ay20

Correct citation for this publication:

Xu, J., Moors-Murphy, H.B., and Vanderlaan A.S.M. 2025. Passive Acoustic Detection of North Atlantic Right Whales in the Cabot Strait: Ambient Noise Analysis and Detection Range Modelling. Can. Tech. Rep. Fish. Aquat. Sci. 3741: vi + 58 p. https://doi.org/10.60825/r9a8-ay20

CONTENTS

ABSTRACT

Xu, J., Moors-Murphy, H.B., and Vanderlaan A.S.M. 2025. Passive Acoustic Detection of North Atlantic Right Whales in the Cabot Strait: Ambient Noise Analysis and Detection Range Modelling. Can. Tech. Rep. Fish. Aquat. Sci. 3741: vi + 58 p. https://doi.org/10.60825/r9a8-ay20

North Atlantic right whales (NARWs) occur throughout most of the Northwest Atlantic from Florida to Newfoundland, with aggregations documented in the Gulf of St. Lawrence in spring, summer and fall in recent years. As they migrate between southern breeding grounds and northern feeding areas, the Cabot Strait serves as a critical movement corridor. This study examines the feasibility of using Passive Acoustic Monitoring (PAM) to detect NARWs as they traverse this high-traffic shipping corridor, with a focus on detecting their contact calls (upcalls). A sparse array of PAM systems was deployed at six mooring stations across the 110 km-wide Cabot Strait from October 2022 to August 2023. Detection distances for NARW upcalls were estimated by using in situ ambient noise level measurements with integrated ocean-acoustic modelling. Detection modeling, based on a 155 dB source level and a 3 dB Signal-to-Noise Ratio (SNR) threshold, was conducted using both quantile and logarithmic regression methods, with quantile regression proving to be the more robust approach. The findings reveal substantial variation in ambient noise levels among the stations. Notably, stations CS2 and CS3, located closest to a shipping lane, exhibited the shortest median detection ranges (5 to 6 km), whereas station CSE achieved the longest median detection range (20 to 25 km), attributable to its generally lower ambient noise levels. The high volume of vessel traffic, with over 20 ships traversing the strait daily, contributes to continuous low-frequency noise in this area, which can propagate up to 100 km, complicating detection efforts. Additionally, seasonal sound channels were observed to enhance sound propagation, but their transient nature underscores the need for adaptive deployment strategies. This study provides a preliminary estimate of NARW detection distances in a complex ocean-acoustic environment, emphasizing the impact of shipping noise on detection effectiveness and highlighting the need for further research to refine PAM-based NARW monitoring strategies in the Cabot Strait.

RÉSUMÉ

Xu, J., Moors-Murphy, H.B., and Vanderlaan A.S.M. 2025. Passive Acoustic Detection of North Atlantic Right Whales in the Cabot Strait: Ambient Noise Analysis and Detection Range Modelling. Can. Tech. Rep. Fish. Aquat. Sci. 3741: vi + 58 p. https://doi.org/10.60825/r9a8-ay20

Les baleines noires de l'Atlantique Nord (BNAN) sont présentes dans la majeure partie du nord-ouest de l'Atlantique, de la Floride jusqu'à Terre-Neuve, avec des agrégations documentées dans le golfe du Saint-Laurent au printemps, en été et en automne au cours des dernières années. Lors de leur migration entre les aires de reproduction du sud et les zones d'alimentation du nord, le détroit de Cabot constitue un corridor de déplacement essentiel. Cette étude évalue la faisabilité d'utiliser la surveillance acoustique passive (SAP) pour détecter les BNAN pendant leur traversée de ce corridor maritime très fréquenté, en se concentrant sur la détection de leurs appels de contact ("upcalls"). Un réseau clairsemé de systèmes SAP a été déployé à six stations d'ancrage à travers le détroit de Cabot, large de 110 km, d'octobre 2022 à août 2023. Les distances de détection des "upcalls" de BNAN ont été estimées à l'aide de mesures in situ du niveau de bruit ambiant et de modélisation acoustique océanique intégrée. La modélisation de la détection, basée sur un niveau source de 155 dB et un seuil de rapport signal/bruit (RSB) de 3 dB, a été réalisée à l'aide des méthodes de régression quantile et régression logarithmique, la régression quantile s'avérant la plus robuste. Les résultats révèlent une variation importante des niveaux de bruit ambiant selon les stations. Notamment, les stations CS2 et CS3, situées au plus près d'un couloir de navigation, ont présenté les distances médianes de détection les plus courtes (5 à 6 km), tandis que la station CSE a obtenu la distance médiane de détection la plus longue (20 à 25 km), ceci étant attribuable à ses niveaux de bruit ambiant généralement plus faibles. Le volume élevé du trafic maritime, avec plus de 20 navires traversant le détroit chaque jour, génère un bruit continu de basse fréquence dans la région, pouvant se propager jusqu'à 100 km, ce qui complique les efforts de détection. De plus, la présence saisonnière de canaux sonores améliore la propagation du son, mais leur nature transitoire souligne le besoin de stratégies de déploiement adaptatives. Cette étude fournit une estimation préliminaire des distances de détection des BNAN dans un environnement océanique-acoustique complexe, en mettant en évidence l'impact du bruit des navires sur l'efficacité de la détection et l'importance de recherches supplémentaires afin de raffiner les stratégies de surveillance SAP des BNAN dans le détroit de Cabot.

1 INTRODUCTION

North Atlantic right whales (NARWs; *Eubalaena glacialis*) occur throughout waters off eastern Canada, and since at least 2015 large aggregations have been documented in the southern Gulf of St. Lawrence (GSL) in the spring, summer and fall (Cole et al. 2020; Crowe et al. 2021;Ratelle and Vanderlaan et al. 2025). Concurrently, increased detections of NARW upcalls using passive acoustic monitoring (PAM) were recorded in the southern Gulf of St. Lawrence (Simard et al. 2019, 2024; Durette-Morin et al. 2022; St-Pierre et al. 2024).

This increased presence of NARWs in the GSL led to more entanglements and vessel strikes due to heavy shipping traffic and fishing activity in the area (Daoust et al. 2017; Bourque et al. 2020). In response, the Government of Canada implemented new management measures in the GSL, including mandatory and voluntary vessel speed limits to reduce vessel strike risk (Transport Canada 2025) and temporal fishing closures to reduce entanglement risk (Fisheries and Oceans Canada 2025). Furthermore, NARW monitoring efforts efforts off eastern Canada have substantially increased (Ratelle and Vanderlaan et al. 2025).

The Cabot Strait, located between Nova Scotia and Newfoundland, serves as the most direct route for NARWs entering the Gulf of St. Lawrence from more southern areas and is considered the main movement corridor for NARWs into the GSL (Ratelle and Vanderlaan et al. 2025). Major shipping lanes also run through this corridor, and in addition to supporting whale movements into and out of the GSL, it is also a critical route for maritime traffic. Monitoring this area, where NARWs and vessels overlap, is important for understanding potential risks to NARWs so that effective protection measures can be implemented.

PAM systems have been extensively utilized to detect and study baleen whales, which communicate, navigate, and interact socially through low-frequency vocalizations. For NARWs, the primary contact call, known as the upcall, is frequently used within PAM studies to detect and classify their presence. The upcall is a frequency-modulated signal that typically begins near 50–100 Hz and sweeps upward to 150–250 Hz over 0.5 to 2 seconds (Parks and Tyack 2005;

Matthews and Parks 2021). PAM studies focused on assessing NARW upcall presence have been used to study the habitat use, seasonal occurrence, distribution, and movement patterns of NARWs off eastern Canada. For example, PAM studies show that NARWs are acoustically detected in waters off Nova Scotia throughout the year, with peak acoustic occurrence in the Bay of Fundy and along the Scotian Shelf reported in fall (Davis et al. 2017; Durette-Morin et al. 2022; Moors-Murphy et al. 2025). Acoustic presence in the GSL occurs from April to December with most detections occurring between June and October (Simard et al. 2019, 2024), while very few acoustic detections (and visual sightings) have been documented off Newfoundland and Labrador (Lawson et al. 2025). Some PAM efforts have occurred in the Cabot Strait area; however, generally very few NARW upcalls have been detected on recordings collected from this area (Moors-Murphy et al. 2025). It is unclear if the limited number of acoustic detections in this area were a result of high noise levels limiting the detection range of the PAM systems and area effectively being monitored or potentially masking received NARW upcalls, or if the low number of upcall detections were due to other factors such as NARW calling behavior (e.g., reduced upcall production) when transiting through areas (Moors-Murphy et al. 2025).

Department of Fisheries and Oceans Maritimes Region has been leading a multi-year research project (with data collection occurring over the period of 2022-2025) aimed at examining immigration and emigration patterns of NARWs through the Cabot Strait. This initiative compiles data from various platforms and explores the spatial and temporal patterns of NARWs as they transit this corridor. Data collected from bottom-moored PAM systems are included as part of this broader project.

The primary objective of this study was to estimate the effective detection distances of NARW upcalls for the PAM systems deployed across the Cabot Strait as part of the broader immigration-emigration study. This analysis primarily focuses on data collected from October 2022 to August 2023 at six stations. Estimating ambient noise levels from measurements and determining effective detection distances at the various mooring locations are essential for assessing the performance of these PAM systems, and for interpreting results from assessment of NARW upcall presence on PAM data sets collected from this area.

The report is structured as follows: Section 2 Data and Materials – Description of the data used for detection distance modelling, PAM system deployments, and data collection. Section 3: Methods - Acoustic Data Analysis and Detection Distance Modeling – Procedures and methods for analyzing acoustic data and estimating detection distances. Section 4: Discussion and Summary – Interpretation of results and key conclusions.

2 DATA AND MATERIALS

2.1 Automatic Identification System Data

The Automatic Identification System (AIS) is a maritime tracking technology that utilizes very high frequency (VHF) radio signals to continuously transmit real-time vessel information, including position (latitude and longitude), speed, course, heading, navigation status, vessel type, name, International Maritime Organization (IMO) number, destination, and estimated time of arrival. The AIS raw data used in this analysis is archived daily through the Canadian Coast Guard data system, and processed using a Python-based decoding package (Guo et al. 2023).

2.2 Bathymetry Data

The bathymetry data used in the model is from a global surface relief model at 15 arc second (Tozer et al. 2019). The bathymetry is produced using a combination of shipboard soundings and depths predicted using satellite altimetry.

2.3 Geoacoustic Data

The geoacoustic properties of the seabed are primarily sourced from historical databases provided by Natural Resources Canada, along with previously published studies (Cameron et al. 1988; Hamilton 1972). The specific values utilized in the acoustic propagation model are detailed in Table 1.

2.4 Wind Data

Wind data used in this analysis is from the High-Resolution Deterministic Prediction System (HRDPS), a high-resolution numerical weather prediction (NWP) model with data assimilation developed and maintained by Environment and Climate Change Canada (ECCC) (Milbrandt et al. 2016). It provides short-term, high-resolution weather forecasts over Canada and adjacent areas. It includes many variables: temperature, wind, precipitation, cloud cover, pressure, and more. The wind data used in this analysis has 2.5 km grid spacing and provides hourly averaged wind speed and direction.

2.5 Reanalysis Ocean Circulation Data

Global Ocean Reanalysis and Simulation (GLORYS) is a series of ocean reanalysis products that assimilate observational data, including both satellites and in situ measurements, into ocean circulation models to provide a detailed, high-resolution representation of past and present ocean conditions (Jean-Michel et al. 2021; Lellouche et al. 2018). Ocean reanalysis, more broadly, is a methodology that integrates observational data with ocean circulation models through systematic data assimilation techniques, producing comprehensive estimates of the historical state of the ocean. These reanalysis products are essential for monitoring, validation, and for improving our understanding of ocean variability and long-term changes (Balmaseda et al. 2013). The GLORYS dataset features a horizontal spatial resolution of $1/12^o$ (approximately 8 km) and includes 50 standard vertical levels, allowing for detailed analysis of ocean variability across different depths. In this study, daily-averaged three-dimensional temperature and salinity fields from GLORYS were utilized to construct a 3-D sound speed field, which served as input for the sound propagation modelling.

2.6 Passive Acoustic Monitoring System and Data

The Cabot Strait plays a significant role in regional circulation, water mass exchange, and climate dynamics (El-Sabh 1977). The water column usually presents seasonal stratification with warmer, fresher surface waters in summer and deep, cold Atlantic waters below (Rousseau et al. 2025); in contrast, winter conditions are characterized by much colder surface waters and increased vertical mixing, resulting in a more weakly stratified water column throughout the passage. Cabot Strait is also characterized by strong tidal currents and a complex interplay between barotropic (surface) and baroclinic (internal) tides, influenced by the region's bathymetry (Han et al. 1999; Hebert 2023). The design and placement of the PAM moorings were primarily guided by the need to reduce flow-introduced mooring noise and minimize exposure to heavy shipping traffic, while ensuring optimal monitoring coverage across the strait. Figure 1 shows the mooring locations in the Cabot Strait, overlaid on a vessel density map. The vessel density is estimated using the method proposed in Falco et al. (2019) and represents the average time percentage of vessel per square km.

Six PAM-equipped moorings were deployed on October 15, 2022, at the following stations: Cape Breton North (CBN), Cabot Strait West (CSW), Cabot Strait 1 (CS1), Cabot Strait 2 (CS2), Cabot Strait 3 (CS3), and Cabot Strait East (CSE). These moorings were later recovered between August 18 and 20, 2023(Table 2). A Seabird MicroCAT SBE37 was configured and deployed alongside each PAM system to collect in situ measurements of temperature, conductivity, and pressure at all deployment stations.

PAM data were collected using Autonomous Multichannel Acoustic Recorders (AMAR; JASCO Applied Sciences, Canada) configured in several different ways at these stations. A four-channel AMAR G4 was deployed on the CBN mooring, configured as a vertical line array with the four hydrophones spaced 10 meters apart and extending from 140 to 170 m depth in the water column. The CSW mooring included an M20 3D particle velocity sensor (GeoSpectrum Technologies Inc., Canada) integrated with a AMAR G4 with hydrophone positioned at approximately 88 m depth. For the CS1, CS2, and CS3 moorings, a single hydrophone integrated with the AMAR UD G4

system was used, with sensors placed at depths ranging from 440 to 490 m. The CSE mooring was equipped with two SoundTrap ST600s (Ocean Instruments, New Zealand), with the hydrophones placed at approximately 155 m depth.

The M20 sensor on the CSW mooring station malfunctioned, and no data were recorded during the deployment period. Additionally, the four-channel hydrophone system at the CBN mooring station experienced an intermittent connection issue between the hydrophone sensors and cables at the start of the deployment. This led to a significant amount of electronic noise, which persisted during the initial weeks of the deployment but gradually improved over time. After examining the complete dataset from this four-channel system, Channel 4 was selected for this study due to its minimal electronic noise contamination.

The coordinates of the mooring stations, along with the hydrophone system models, system sensitivity, and sampling frequencies, are provided in Table 2. Note that the AMAR UD G4 single-hydrophone systems deployed at CS1, CS2, and CS3 collected data at two different sampling frequencies (128 kHz and 256 kHz) over different duty cycles. However, for this study, only the 128 kHz sampling data were used.

3 METHODS

3.1 Acoustic Data Analysis

3.1.1 Ambient Noise Measurement and Estimation

Sound pressure levels across various one-third octave bands[International Electrotechnical Commission (2014); American National Standards Institute (2004)] were calculated from the collected data. Since ambient noise analysis and detection range modeling primarily focus on low-frequency bands (<1 kHz), the waveform data from CS1, CS2, CS3, and CSE were downsampled to 16 kHz to optimize processing efficiency. The acoustic data were then processed using short time Fast Fourier Transform (SFFT) to estimate sound pressure levels across different frequencies and

time. The FFT length was 8092, utilizing Hann window 50% overlap. This resulted in a spectrogram with approximately a 0.25-second resolution in time and a 2-Hz resolution in frequency (Figures 2 to 7, bottom panels).

Relative Spectral Probability Density (RSPD) is a method used to statistically describe the distribution of power spectra density (PSD) values across a range of frequencies over time. Instead of presenting a single PSD estimate, RSPD shows the relative occurrence of different power levels at each frequency over a given time period. This helps differentiate persistent and transient acoustic features (McNamara and Buland 2004; Parks et al. 2009; Merchant et al. 2013).

If $S(f,t)$ represents the short-term power spectra density at frequency f and time t, then the RPSD is given by :

$$P(S \mid f) = \frac{N(f)}{N(S,f)}, \tag{1}$$

where $N(S,f)$ is the number of occurrences of a given PSD level S at frequency f; and $N(f)$ is the total number of PSD observations at frequency f.

RSPD plots were generated for each dataset and overlaid with different percentile PSD values and the Wenz (Wenz 1962) spectrum limit (Figures 2 to 7, upper panels).

3.1.2 Wind Data and its Correlation with SPL

Wind-generated underwater noise primarily results from breaking waves, which create air bubbles that, as they oscillate and collapse underwater, produce acoustic energy within the water column (Ma et al. 2005). Typically, underwater noise is dominated by wind-induced sources in the frequency range of 400 Hz to 50 kHz, while lower frequencies are more influenced by anthropogenic activities (Wenz 1962; Hildebrand 2009). In the wind-dominated frequency range, noise levels are expected to correlate well with wind speed [Hildebrand et al. (2021)]. Therefore, analyzing the correlation between sound pressure level (SPL) and wind speed helps assess whether the recorded data are primarily influenced by environmental noise or contaminated by additional sources.

To investigate this relationship, the High-Resolution Deterministic Prediction System (HRDPS) datasets from Environment and Climate Change Canada were utilized. The model grid point closest to each mooring location represents local atmospheric conditions. Correlation coefficients between the hourly minimum, maximum, and average SPL across 1/3 octave bands and wind speed were calculated to evaluate the relationship between wind speed and underwater noise levels (Figure 27).

3.2 Integrated Ocean-Acoustic Modelling

An integrated ocean-acoustic approach of detection range modelling was implemented for the five PAM locations, where PAM data were successfully collected from October 2022 to August 2023. High-fidelity ocean circulation models are increasingly used to support acoustic modeling because they provide detailed and realistic environmental conditions that influence underwater sound propagation. These models simulate dynamic oceanographic processes such as temperature, salinity, currents, and stratification, all of which impact sound speed in the water column and acoustic transmission loss (TL) (Lermusiaux et al. 2010; Duda et al. 2019).

TL was computed using a range-dependent normal mode numerical solution, integrated with a best-estimate 3D sound speed field derived from reanalysis global ocean circulation model data. The omnidirectional propagation of a continuous-wave (CW) signal at 100 Hz was estimated using an Nx2D sound propagation framework. In this approach, sound propagation from the source to receivers (hydrophones) was simulated within a 2D vertical slice, and the simulation was then repeated at fixed azimuthal intervals (10 degree for this study) to construct the full Nx2D sound propagation field.

3.2.1 Extract Bathymetry Data from Global Surface Relief Model

The first step of modelling was to extract the bathymetry profile along the geometric propagation path between the source and receiver(specifically, the great circle path along the Earth's surface)

from the global 15-second bathymetry model, as shown in Figure 9a. A propagation distance of 120 km was selected to ensure it extends well beyond the potential propagation range of NARW upcalls (i.e. the distance a 100 Hz continuous wave signal is able to travel before it drops below the ambient noise level).

3.2.2 3D Sound Speed Field Constructed from Reanalysis Ocean Circulation Data

After defining the geometric propagation path between the source and receiver, the Nx2D temperature and salinity fields along this path were extracted by interpolating from the 3D reanalysis ocean circulation model data. These environmental fields were subsequently used to compute the sound speed profile for acoustic propagation modelling. An example of the original temperature and salinity fields along a 2D slice of the acoustic propagation path is shown in Figure 10. The sound speed was then estimated using the formulation defined in IOC and IAPSO (2010) and implemented in the Python package (McDougall and Barker 2011)(e.g. Figure 11).

3.2.3 Acoustic Propagation Model and Transmission Loss Estimation

The reciprocity principle was applied in the modeling setup, representing the symmetry in propagation between a source and receiver when their positions are exchanged (Kinsler et al. 2000). Instead of estimating sound propagation loss from all potential NARW call sources at different locations to the PAM system mooring, TL was estimated using a virtual sound source at the PAM location.

Coupled SACLANTCEN Normal Mode Propagation Loss Model (C-SNAP) was used to calculate TL (Ferla et al. 1993). C-SNAP is based on SACLANTCEN range-independent normal mode program (SNAP). Range-dependence is constructed by dividing the propagation path into a sequence of range-independent segments.

Assuming that the acoustic field is dominated by the outgoing component,

$$p(r,z) = \frac{i}{4\rho(z_s)} \sum_{m=1}^{\infty} \Psi_m(z_s)\Psi_m(z)H_0^1(k_m r), \tag{2}$$

where r is the range, z is the depth, ρ is density, z_s is the source depth, Ψ_m is the mode amplitude, H_0^1 is the zero-order Hankel function of the first kind,k_m is the eigenvalue.

Figure 12 illustrates an example of this sound propagation modelling with C-SNAP. On the upper panel, it shows TL as function of depth and distance from 100 Hz sound source at depth of 457 m. The lower panel shows the average TL as function of distance of first 60 m depth average and the TL at depth of mooring location. It shows significant sound attenuation during up-slope propagation due to bottom attenuation.

TL was estimated at 10-degree intervals in the azimuthal direction along the circle (Figure 9a). Figure 13 shows sound propagation simulations for four azimuthal directions at CSW, illustrating how complex bathymetry affected sound propagation condition.

A similar procedure was applied to all stations. To estimate the TL of upcalls signal in all directions, the TL was averaged over the first 60 meters of water depth, since NARWs typically vocalize at depths less than 20 m (Parks et al. 2019). Figure 14 presents these average TL values at distance of 20 km for all six stations for November 15, 2022.

3.3 Detection Distance Modelling Setup

3.3.1 Passive Acoustic Detection based on SONAR Equation

Passive acoustic detection relies on the principles of the sonar equation to estimate the detectability of underwater sound sources. It involves listening for sounds underwater, such as those produced by marine mammals (e.g. upcalls) and other natural sources, as well as those originating from vessels and human activity. The fundamental sonar equation for passive detection is

$$SL - TL - NL + DI = SNR, \tag{3}$$

where SL (Source Level) represents the intensity of the sound emitted by the source, TL (Transmission Loss) accounts for the attenuation of sound as it propagates through the water, NL (Noise Level) includes background environmental and system noise, and DI (Directivity Index) quantifies the ability of a directional hydrophone to reduce noise. For the omnidirectional hydrophone that was used in this study, the DI was zero. SNR (Signal-to-Noise Ratio) represents the difference between the received signal level and the background noise level. It is a measured value that determines how much the signal stands out from noise.

Detection Threshold (DT) is a predefined system parameter that specifies the minimum SNR required for reliable detection.

In the passive sonar equation, the detection criterion is expressed as:

$$SNR \geq DT, \tag{4}$$

For NARWs, the upcall frequency band typically ranges from 63 to 250 Hz with a minimum SL of 146 dB, an average of 150 dB, and a maximum 155 dB (Parks and Tyack 2005). In this study, the DT was set to 3 dB, and 100 Hz was chosen as the representative frequency for NARW upcall detection.

3.4 Regression Method to Derive Detection Distance

In acoustic detection range modelling, the passive SONAR equation relates key acoustic variables (e.g. SL,TL,NL,SNR) to estimate the distance at which a target can be detected. However, in complex underwater environments, TL does not have a simple, direct mathematical relationship with distance, as it is influenced by many factors such as water depth, temperature, salinity, bottom characteristics, and frequency. Typically, TL follows an empirical or theoretical decay pattern with increasing distance, which can be modeled using regression techniques. By applying regression to empirical data of TL at various known distances, it becomes possible to more accurately and practically estimate detection range when using the SONAR equation, especially in situations where

theoretical models are insufficient to represent real underwater conditions.

3.4.1 Logarithmic Regression (Empirical TL Models)

Logarithmic regression is commonly used to model two variables following a diminishing return pattern:

$$Y = \beta_0 + \beta_1 \log(X) + \epsilon, \tag{5}$$

where $\log(X)$ is the natural logarithm of X.

As for the modelling of transmission loss as function of distance, it follows the form:

$$TL = TL_0 + 10n \log_{10}(d), \tag{6}$$

where TL is the transmission loss at distance d, TL_0 is a reference loss (often near the source), and n is the spreading coefficient. In theory, without considering reflection from the surface and bottom, $n = 10$ for cylindrical spreading, $n = 20$ for spherical spreading, and d is the distance from the source. A log-log regression is often used to fit this equation, estimating n and TL_0 (Marques et al. 2013; Küsel et al. 2011). Once a TL vs distance regression model is fitted, detection range is estimated using

$$TL(d_{det}) = SL - NL + DI - DT, \tag{7}$$

By solving for d_{det} using the regression model, the estimated detection range is obtained. A similar approach and application has been demonstrated in Wingfield et al. (2022).

Figure 15 presents examples of the logarithmic regression model fitted to TL as a function of distance, based on sound propagation modeling results for CS3. However, as shown in Figure 15b, not all regression models provide a good fit to the data.

3.4.2 Quantile Regression (For Noise-Dependent TL Variability)

In contrast to logarithmic regression models, quantile regression offers a different statistical framework for characterizing the relationship between two variables. It estimates conditional quantiles (e.g., median or other percentiles) of the response variable rather than the mean. It is useful when the relationship between variables varies across different quantiles. If TL varies due to environmental factors (e.g., multipath propagation, variable seabed absorption), quantile regression can be applied to estimate different percentiles of TL vs. distance:

$$Q_\tau(Y \mid X) = \beta_0 + \beta_1 X, \tag{8}$$

where Q_τ represents the quantile function at level τ.

An example demonstrating the improved robustness of the quantile regression method compared to the logarithmic regression model is shown in Figure 16. In Figure 16a, the logarithmic regression estimate (green dot or bar) closely aligns with the 50th percentile (median) of the quantile regression method. However, in Figure 16b, the logarithmic regression model overestimates the detection distance compared to the quantile regression method, which provides a more reasonable estimate based on the TL results shown in the right-column panels, indicated by the blue lines.

4 RESULTS AND DISCUSSION

4.1 Detection Distance Modeling and Analysis

The SONAR equation indicates that, when the SL and frequency are fixed, the dominant factors influencing the detection range of upcalls are TL and NL. These parameters largely determine the effective range at which upcalls can be detected above background noise. For this study, TL was determined as the average propagation loss between the water surface and 60 m depth, consistent with the assumption that NARW calls originate within these depths.

NL was determined from in situ measurement. Figure 8 shows the hourly averaged NL of the frequency band from 80 to 105 Hz for the month of November 2022 for the five stations with available data. Among the five stations, CBN exhibited the highest NL. This was likely due to system self-noise caused by a potential malfunction of the hydrophone system. As shown in Figure 2, a significant amount of electronic noise was present during the first few days of the CBN deployment. In the RSPD analysis, PSD values above the 95th percentile were primarily attributed to this electronic noise. This noise is believed to have resulted from the conductor being stretched beyond its designed limit. Interestingly, after a few weeks, the system appeared to reach an equilibrium state, leading to a substantial reduction in electronic noise. However, this issue may have introduced measurement errors throughout the dataset.

For all other stations, there were considerable variations in ambient noise levels, exceeding 25 dB across most frequency bands. In the 10 Hz to 1 kHz range, ambient noise was predominantly influenced by shipping traffic. In contrast, within the 100 Hz to 8 kHz band, wind noise was the dominant contributor, with its influence increasing with frequency. The deep-water stations CS1, CS2, and CS3 followed similar trends, with CS3 showing slightly higher noise levels due to its proximity to the shipping lane (Figure 1). Among all stations, CSE had the lowest noise level (Figure 6, 7).

The detection distance for all stations was estimated using the SONAR equation, in situ NL, and regression methods for November 2022. The simulation was limited to November 2022 for several reasons. These include high computational cost, an initial focus on exploring NARWs detection distances across Cabot Strait moorings, and previous PAM studies indicating that most detections occur during the fall (Moors-Murphy et al. 2025). This estimation was performed for all azimuthal directions at each station. In Figures 17 to 21, the detection distance as a function of time is shown for a single, representative azimuthal direction at each station. In these estimations, TL was calculated using a sound speed profile that is fixed in time but range-dependent, along with bathymetry for each azimuthal direction. The sound speed profile was assumed constant from day to day. Consequently, the variation in detection range was primarily driven by the significant daily fluctuations in ambient noise levels. It can be observed that the detection distance was inversely

proportional to the ambient noise level over time.

The monthly average detection distance of NARW upcalls for November 2022 is shown in Figure 22 for the five stations with available in situ NL measurement data. The blue line represents the results from the logarithmic regression model, while the red line corresponds to the modified quantile regression model.

For the quantile regression model, among the three deep stations (CS1, CS2, and CS3), CS2 and CS3 exhibited the shortest detection distances, ranging from approximately 4 to 6 km. This result aligns with previous analyses, which indicate that CS2 and CS3 experienced slightly higher ambient noise levels due to their closer proximity to the shipping lane compared to the other stations. In contrast, the CSE station exhibited the longest detection distance, primarily because of its lower ambient noise levels relative to the other stations.

It should be noted that there are significant variations in the logarithmic regression model results (blue lines) along the azimuthal directions for each station. These variations are attributed to the non-robust nature of the regression model for this particular case, which introduces errors in the detection distance estimations. Given the similar propagation conditions for these deep stations, such large variations are unexpected. Recognizing the limitations and errors of the logarithmic regression model led to the adoption of a modified quantile regression model in this study.

Figure 23 shows the 50th percentile detection distance estimation for each station projected onto the map of Cabot Strait. Note that the CSW station is not estimated due to missing in situ NL data. These PAM moorings provide extensive coverage across the Cabot Strait, validating the original design and configuration of the PAM mooring system's deployment. However, it is important to note that spatial coverage of the area is incomplete and varies over time.

4.2 Shipping Traffic Analysis and Shipping Noise Impact Assessment

The Cabot Strait is an important international shipping route, serving as the primary waterway linking the Atlantic Ocean with inland ports on the Great Lakes and the St. Lawrence Seaway.

With global trade on the rise, shipping traffic is increasing worldwide and expanding into more areas (Tournadre 2014). Therefore, it is useful to quantitatively analyze the number and types of vessels in this busy shipping route. There are routine ferries operating year-round between Sydney, Nova Scotia, and Port aux Basques, Newfoundland. To exclude this well-known traffic, a restricted area is indicated in Figure 24. The vessel traffic information is shown in Figure 25, which provides daily statistics on vessel numbers and types for November 2022; and in Figure 26, which provides monthly statistics on vessel numbers and types for months from January 2022 to March 2023.

The majority of shipping traffic consists of cargo and tanker vessels. The third largest component is fishing vessels, which are only present seasonally. On average, more than 20 vessels pass through the Cabot Strait each day, typically taking at least an hour or more to traverse. This indicates that the area could potentially be continuously sonified throughout the day by both nearby and distant vessels. As shown in Figure 13b, low-frequency vessel noise can transmit up to 100 km with a TL of 70 to 80 dB. Given a typical vessel SL of 160 dB (180 dB or above for large cargo or tanker), the residual sound level could still be above the ambient noise level after propagating 100 km. With the continuous presence of vessel noise, both from nearby and distant sources, achieving a noise-free environment for monitoring will be difficult.

4.3 Wind-Induced Noise and Mooring Self-Noise

Figure 27 shows the correlation coefficients between the hourly minimum, maximum, and average SPL across 1/3 octave bands and wind speed for each station over the whole deployment period.

For all stations, the background noise, represented by the minimum SPL, in the frequency band from 400 Hz to 5 kHz showed a strong correlation with wind. The maximum SPL from low frequencies (10 Hz) to 1 kHz was usually still influenced by nearby vessel noise. The peak around 1 kHz for the deep stations (CS1, CS2, and CS3) indicates that wind played a role in increasing the SPL. The complete lack of correlation between the maximum SPL and wind at CBN suggests erratic measurements by the PAM system as discussed in previous. Note that the sudden decrease around

8 kHz for CS1, CS2, CS3, and CSE was caused by low-pass filtering during the downsampling process.

4.4 Implications for PAM Based Whale Monitoring

In the passive acoustic SONAR equation [3], once the SL and detection threshold are set, detection performance is primarily influenced by TL and NL. Improving detection requires reducing both NL and TL. One approach is optimizing the hydrophone's location to minimize ambient noise levels. However, in practice, reducing PAM self-noise or mitigating motion-induced pseudo-noise caused by currents is challenging. Another strategy is positioning the hydrophone in the optimal receiving spot to maximize signal reception, effectively minimizing TL.

In a stratified ocean, there is typically a layer where sound waves can propagate over long distances with minimal attenuation, due to the combined effects of temperature, pressure, and salinity on sound speed. This layer is commonly referred to as the sound channel. The most well-known is the Deep Sound Channel (DSC), also known as the SOFAR (Sound Fixing and Ranging) Channel, which is typically found at depths between 600–1200 meters (Hale 1961). In shallow oceans, similar sound channels can also form under certain oceanographic conditions. The top panel of Figure 28a shows a sound channel at a depth of approximately 75 meters in November 2022. Placing a PAM system at this depth layer (60 m), assuming the same noise level as at the original 457-meter depth, could enhance detection performance. Figure 28 illustrates the favorable sound propagation conditions when the sound source is at a depth of 60 meters (Figure 28b) compared to 457 meters (Figure 28c). Figure 29 shows the detection distance using a PAM system deployed at a depth of 60 m, assuming the same background noise level as at a depth of 457 m. The detection distance has improved from the original 6-8 km (Figure 22d) to 10-12 km.

However, this seasonal sound channel may change or even disappear in different months. To adaptively take advantage of this seasonal sound channel, a mooring system with PAM that can be lifted up and sunk down according to the sound channel depth is ideally preferred. An array system with a multi-sensor setup could also be used to increase the SNR. While these are all possible with

current technology being developed or commercialized, this is beyond the scope of this study.

In this study, sound propagation and detection range modeling were conducted using a single representative frequency of 100 Hz and a maximum upcall SL of 155 dB, rather than the average SL of 150 dB. This choice was made to assess the upper limit of the system's detection range, rather than the typical range achievable under average conditions. Together with a detection threshold of 3 dB, these modeling parameters characterize the best-case scenario for detection distance in a highly complex acoustic environment. While, in reality, the upcall is a broadband signal spanning from 63 to 250 Hz, and SL can vary with individual and environmental conditions, this modeling approach provides a simplified estimate of detection range. In the regression analysis, a quantile regression approach was used with a 1.5 dB perturbation from the detection threshold. This 1.5 dB value is somewhat arbitrary. Future work should address these limitations by employing a Monte Carlo simulation approach that randomizes parameters such as SL, frequency band, geo-acoustic bottom properties, and background sound speed profiles for a more comprehensive assessment.

5 CONCLUSION

In this study, an integrated ocean-acoustic model was used to estimate NARW detection ranges for November 2022. Modeling results, based on the SONAR equation, indicated that transmission loss and ambient noise level were the main factors affecting detection performance. Notably, marked spatial variation in noise was observed: CS2 and CS3, closest to a shipping lane, had the shortest detection range, while CSE exhibited the longest due to reduced noise levels at the mooring site. To more accurately assess detection capabilities, future efforts should implement Monte Carlo simulations that account for uncertainties in source levels, frequency bands, geo-acoustic properties, and background sound speed profiles.

Cabot Strait serves as a major international shipping route. Vessel traffic data reveal that cargo and tanker vessels dominate, while fishing vessels are present primarily on a seasonal basis. On average, over 20 vessels traverse the strait daily, contributing to continuous low-frequency noise that can propagate up to 100 km, making noise-free monitoring challenging. Additionally, seasonal

sound channels can enhance sound propagation; however, their transient nature underscores the need for adaptive deployment strategies.

Using a PAM system to monitor NARWs in the Cabot Strait presents several challenges that limit its effectiveness, as detection relies primarily on upcalls; however, NARWs may vocalize less frequently in migratory corridors or during transit than in feeding or social aggregation areas, which limits detection compared to some other baleen whale species (Mussoline et al. 2012; Murray et al. 2022). This sporadic calling behavior inherently reduces the probability of detection, even when whales are present.

In addition to behavioral factors, the monitoring systems themselves introduce limitations. Spatial coverage of PAM arrays in the Cabot Strait is incomplete and can vary further due to fluctuating levels of ambient noise, particularly during periods of intense shipping activity or inclement weather. Temporally, the use of duty-cycled recordings, implemented to conserve data storage and equipment life, means that some vocalizations occurring within the nominal detection range may be missed. This combination of spatial gaps, temporal gaps, and sporadic calling helps explain the low rate of NARW upcall detections observed in our dataset (Moors-Murphy et al. 2025).

Anthropogenic noise adds another layer of complexity. Cabot Strait span roughly 110 km, is an important international shipping route, being the primary waterway linking the Atlantic with inland ports on the Great Lakes and St. Lawrence Seaway. Shipping noise is undoubtedly one of the major factors to affect the detection of NARWs upcall signals. Noise from vessel traffic is high and variable, often overlapping with the frequencies of NARW calls. Studies have shown that right whales, as well as other baleen whales, may reduce or even cease calling in noisy environments (Parks et al. 2007), which further limits the effectiveness of PAM in this highly trafficked region.

In conclusion, this study provides a preliminary estimate of NARW detection distances in the acoustically complex Cabot Strait and underscores the necessity for further research to optimize PAM-based whale detection within this region.

REFERENCES

American National Standards Institute 2004. ANSI S1.11-2004 Specification for Octave-Band and Fractional-Octave-Band Analog and Digital Filters. American National Standards Institute, Washington, DC, USA. Available: https://webstore.ansi.org/standards/asa/ansis1112004.

Balmaseda, M.A., Mogensen, K., and Weaver, A.T. 2013. The nemovar-combined global ocean reanalysis and its instrumental bias correction. Quarterly Journal of the Royal Meteorological Society **139**(674): 1132–1149. doi:10.1002/qj.2063.

Bourque, L., Wimmer, T., Lair, S., Jones, M., and Daoust, P. 2020. Incident report: North atlantic right whale mortality event in eastern canada, 2019. Collaborative Report Produced by: Canadian Wildlife Health Cooperative and Marine Animal Response Society 209 pp.

Cameron, G., Best, M.A., Fader, G.B., Piper, D., and Pratt, J. 1988. Quaternary geology of the continental margin of eastern Canada. Geological Survey of Canada.

Cole, T.V., Crowe, L.M., Corkeron, P.J., and Vanderlaan, A.S. 2020. North Atlantic right whale abundance, demography and residency in the southern Gulf of St. Lawrence derived from directed aerial surveys. Canadian Science Advisory Secretariat (CSAS).

Crowe, L.M., Brown, M.W., Corkeron, P.J., Hamilton, P.K., Ramp, C., Ratelle, S., Vanderlaan, A.S., and Cole, T.V. 2021. In plane sight: a mark-recapture analysis of north atlantic right whales in the gulf of st. lawrence. Endangered Species Research **46**: 227–251.

Daoust, P.Y., Couture, E., Wimmer, T., and Bourque, L. 2017. Incident report: North atlantic right whale mortality event in the gulf of st. lawrence, 2017. Collaborative report. 256 pp.

Davis, G.E., Baumgartner, M.F., Bonnell, J.M., Bell, J., Berchok, C., Bort Thornton, J., Brault, S., Buchanan, G., Charif, R.A., Cholewiak, D. et al. 2017. Long-term passive acoustic recordings track the changing distribution of north atlantic right whales (eubalaena glacialis) from 2004 to 2014. Scientific reports **7**(1): 13460.

Duda, T.F., Lin, Y.T., Newhall, A.E., Helfrich, K.R., Lynch, J.F., Zhang, W.G., Lermusiaux, P.F., and Wilkin, J. 2019. Multiscale multiphysics data-informed modeling for three-dimensional ocean acoustic simulation and prediction. The Journal of the Acoustical Society of America **146**(3): 1996–2015.

Durette-Morin, D., Evers, C., Johnson, H.D., Kowarski, K., Delarue, J., Moors-Murphy, H., Maxner, E., Lawson, J.W., and Davies, K.T.A. 2022. The distribution of North Atlantic right whales in Canadian waters from 2015-2017 revealed by passive acoustic monitoring. Frontiers in Marine Science **9**: 976044. doi:10.3389/fmars.2022.976044.

El-Sabh, M.I. 1977. Oceanographic Features, Currents, and Transport in Cabot Strait. Journal of the Fisheries Research Board of Canada **34**(4): 516–528. doi:10.1139/f77-083.

Falco, L., Pittito, A., Adnams, W., Earwaker, N., and Greidanus, H. 2019. Eu vessel density map. Detailed method .

Ferla, C.M., Porter, M., and Jensen, F.B. 1993. C-snap: Coupled saclantcen normal mode propagation loss model. Technical report, NATO. SACLANTCEN.

Fisheries and Oceans Canada 2025. Management measures for north atlantic right whales. https://www.dfo-mpo.gc.ca/fisheries-peches/commercial-commerciale/atl-arc/narw-bnan/management-gestion-eng.html. Accessed: 2025-09-24.

Guo, L., Xu, J., Li, S., and Wingfield, J. 2023. A Python package for decoding Automatic Identification System (AIS) data from the Canadian Coast Guard, volume 360. Department of Fisheries and Oceans.

Hale, F. 1961. Long-range sound propagation in the deep ocean. The Journal of the Acoustical Society of America **33**(4): 456–464.

Hamilton, E.L. 1972. Compressional-wave attenuation in marine sediments. Geophysics **37**(4): 620–646.

Han, G., Loder, J.W., and Smith, P.C. 1999. Seasonal-Mean Hydrography and Circulation in the Gulf of St. Lawrence and on the Eastern Scotian and Southern Newfoundland

Shelves. Journal of Physical Oceanography **29**(6): 1279–1301. doi:10.1175/1520-0485(1999)029<1279:SMHACI>2.0.CO;2.

Hebert, D. 2023. Physical oceanographic conditions in the gulf of st. lawrence in 2022. Can. Tech. Rep. Fish. Aquat. Sci. 3500, Fisheries and Oceans Canada.

Hildebrand, J.A. 2009. Anthropogenic and natural sources of ambient noise in the ocean. Marine Ecology-progress Series - MAR ECOL-PROGR SER **395**: 5–20. doi:10.3354/meps08353.

Hildebrand, J.A., Frasier, K.E., Baumann-Pickering, S., and Wiggins, S.M. 2021. An empirical model for wind-generated ocean noise. The Journal of the Acoustical Society of America **149**(6): 4516–4533. doi:10.1121/10.0005430.

International Electrotechnical Commission 2014. IEC 61260-1:2014 Electroacoustics – Octave-band and fractional-octave-band filters – Part 1: Specifications. International Electrotechnical Commission, Geneva, Switzerland. Available: https://webstore.iec.ch/publication/21788.

IOC, S. and IAPSO 2010. The international thermodynamic equation of seawater–2010: Calculation and use of thermodynamic properties. Intergovernmental Oceanographic Commission, UNESCO Manuals and Guides No **56**(203): 196.

Jean-Michel, L., Eric, G., Romain, B.B., Gilles, G., Angélique, M., Marie, D., Clément, B., Mathieu, H., Olivier, L.G., Charly, R. et al. 2021. The copernicus global 1/12 oceanic and sea ice glorys12 reanalysis. Frontiers in Earth Science **9**: 698876.

Kinsler, L.E., Frey, A.R., Coppens, A.B., and Sanders, J.V. 2000. Fundamentals of acoustics. John wiley & sons.

Küsel, E.T., Miller, L.A., Madsen, P.T., Siebert, U., and Wahlberg, M. 2011. Cetacean acoustic detection capability: An example with sperm whales. The Journal of the Acoustical Society of America **129**(3): 1723–1731. doi:10.1121/1.3543958.

Lawson, J., Sheppard, G., Morrissey, K., and Healey, V. 2025. Interim summary of north atlantic right and blue whale calls detected recently in newfoundland and labrador. Technical Report 2025/009, DFO Canadian Science Advisory Secretariat. Iv + 17 p.

Lellouche, J.M., Greiner, E., Le Galloudec, O., Garric, G., Regnier, C., Drevillon, M., Benkiran, M., Testut, C.E., Bourdalle-Badie, R., Gasparin, F., Hernandez, O., Levier, B., Drillet, Y., Remy, E., Desportes, C., and Gehlen, M. 2018. Recent updates to the copernicus marine service global ocean monitoring and forecasting real-time 1/12° high-resolution system. Ocean Science **14**: 1093–1126. doi:10.5194/os-14-1093-2018.

Lermusiaux, P.F., Xu, J., Chen, C.F., Jan, S., Chiu, L.Y., and Yang, Y.J. 2010. Coupled ocean–acoustic prediction of transmission loss in a continental shelfbreak region: Predictive skill, uncertainty quantification, and dynamical sensitivities. IEEE Journal of Oceanic Engineering **35**(4): 895–916.

Ma, B.B., Nystuen, J.A., and Lien, R.C. 2005. Prediction of underwater sound levels from rain and wind. The Journal of the Acoustical Society of America **117**(6): 3555–3565. doi:10.1121/1.1910283.

Marques, T.A., Thomas, L., Simpson, S.L., Borchers, D.L., Marques, P.J., Petersen, K.P., and Harwood, J. 2013. Estimating animal population density using passive acoustics. Biological Reviews **88**(2): 287–309. doi:10.1111/brv.12001.

Matthews, L.P. and Parks, S.E. 2021. An overview of north atlantic right whale acoustic behavior, hearing capabilities, and responses to sound. Marine Pollution Bulletin **173**: 113043. doi:https://doi.org/10.1016/j.marpolbul.2021.113043.

McDougall, T.J. and Barker, P.M. 2011. Getting started with TEOS-10 and the Gibbs Seawater (GSW) Oceanographic Toolbox. SCOR/IAPSO WG127.

McNamara, D.E. and Buland, R.P. 2004. Ambient noise levels in the continental united states. Bulletin of the seismological society of America **94**(4): 1517–1527.

Merchant, N.D., Barton, T.R., Thompson, P.M., Pirotta, E., Dakin, D.T., and Dorocicz, J. 2013. Spectral probability density as a tool for ambient noise analysis. The Journal of the Acoustical Society of America **133**(4): EL262–EL267.

Milbrandt, J.A., Bélair, S., Faucher, M., Vallée, M., Carrera, M.L., and Glazer, A. 2016. The pan-canadian high resolution (2.5 km) deterministic prediction system. Weather and Forecasting **31**(6): 1791–1816.

Moors-Murphy, H., Macklin, G., Evers, C., Stanistreet, J., Colbourne, N., Wingfield, J., Xu, J., and Vanderlaan, A. 2025. Acoustic occurrence of north atlantic right whales (eubalaena glacialis) from 2017-2022 off nova scotia. Can. Sci. Advis. Sec. Res. Doc. **in press**: 44.

Murray, A., Rekdahl, M.L., Baumgartner, M.F., and Rosenbaum, H.C. 2022. Acoustic presence and vocal activity of north atlantic right whales in the new york bight: Implications for protecting a critically endangered species in a human-dominated environment. Conservation Science and Practice **4**(11): e12798.

Mussoline, S.E., Risch, D., Hatch, L.T., Weinrich, M.T., Wiley, D.N., Thompson, M.A., Corkeron, P.J., and Van Parijs, S.M. 2012. Seasonal and diel variation in north atlantic right whale up-calls: implications for management and conservation in the northwestern atlantic ocean. Endangered Species Research **17**: 17–26.

Parks, S.E. and Tyack, P.L. 2005. Sound production by north atlantic right whales (eubalaena glacialis) in surface active groups. The Journal of the Acoustical Society of America **117**(5): 3297–3306.

Parks, S.E., Clark, C.W., and Tyack, P.L. 2007. Short-and long-term changes in right whale calling behavior: The potential effects of noise on acoustic communication. The Journal of the Acoustical Society of America **122**(6): 3725–3731.

Parks, S.E., Urazghildiiev, I., and Clark, C.W. 2009. Variability in ambient noise levels and call parameters of north atlantic right whales in three habitat areas. The Journal of the Acoustical Society of America **125**(2): 1230–1239.

Parks, S.E., Cusano, D.A., Johnson, M., Nowacek, D.P., and Tyack, P.L. 2019. North atlantic right whale (eubalaena glacialis) acoustic behavior on the calving grounds. Marine Mammal Science **35**(1): 206–224.

Ratelle, S., Vanderlaan, A., Thompson, E., Sorochan, K., Pisano, O., and Labbé, A. 2025. Important habitats of the north atlantic right whale (*Eubalaena glacialis*) in eastern canadian waters. Technical Report 2025/059, DFO Canadian Science Advisory Secretariat. V + 131 p.

Rousseau, S., Lavoie, D., Jutras, M., and Chassé, J. 2025. Transit time of deep and intermediate waters in the gulf of st. lawrence. Ocean Modelling p. 102526.

Simard, Y., Roy, N., Giard, S., and Aulanier, F. 2019. North Atlantic right whale shift to the Gulf of St. Lawrence in 2015, revealed by long-term passive acoustics. Endangered Species Research **40**: 271–284. doi:10.3354/esr01005.

Simard, Y., Giard, S., Roy, N., Royer, P., Chartrand-Lemieux, M.E., and Perreault, E. 2024. Time-space distribution of north atlantic right whale in gulf of st. lawrence from acoustic monitoring between 2010 and 2022 .

St-Pierre, A.P., Koll-Egyed, T., Harvey, V., Lawson, J.W., Sauvé, C., Ollier, A., Goulet, P.J., Hammill, M.O., and Gosselin, J.F. 2024. Distribution of north atlantic right whales, eubalaena glacialis, in eastern canada from line-transect surveys from 2017 to 2022 .

Tournadre, J. 2014. Global ship traffic and its impact on the marine environment. Nature Geoscience **7**: 101–106. doi:10.1038/ngeo2038.

Tozer, B., Sandwell, D.T., Smith, W.H., Olson, C., Beale, J.R., and Wessel, P. 2019. Global bathymetry and topography at 15 arc sec: Srtm15+. Earth and space science **6**(10): 1847–1864.

Transport Canada 2025. Protecting north atlantic right whales from collisions with vessels in the gulf of st. lawrence. https://tc.canada.ca/en/marine-transportation/navigation-marine-conditions/protecting-north-atlantic-right-whales-collisions-vessels-gulf-st-lawrence. Accessed: 2025-09-24.

Wenz, G.M. 1962. Acoustic ambient noise in the ocean: Spectra and sources. The Journal of the Acoustical Society of America **34**(12): 1936–1956. doi:10.1121/1.1909155.

Wingfield, J.E., Rubin, B., Xu, J., Stanistreet, J.E., and Moors-Murphy, H.B. 2022. Annual, seasonal, and diel patterns in blue whale call occurrence off eastern canada. Endangered Species Research **49**: 71–86.

6 TABLES

Table 1. Geoacoustic properties for the Laurentian Channel used for sound propagation modelling. p-wave stands for compression wave; s-wave stands for shear wave.

Depth (m)	**Material**	**Density (g/cm^3)**	**P-wave speed (m/s)**	**P-wave attenuation (dB/λ)**	**S-wave speed (m/s)**	**S-wave attenuation (dB/λ)**
0-30	Pelite	1.52-1.61	1505-1740	0.44-1.2	120	0.05
30-120	Glacial till	2.0-2.1	2000-2400	1.5-2.2		
120-1000	Sandstone	2.2-2.6	3000-4000	0.05		
> 1000	Sandstone	2.6	4000	0.05		

Table 2. PAM deployment location in Cabot Strait: Cape Breton North (CBN), Cabot Strait West (CSW), Cabot Strait 1 (CS1), Cabot Strait 2 (CS2), Cabot Strait 3 (CS3), and Cabot Strait East (CSE).

Station Name	Latitude (decimal degrees)	Longitude (decimal degrees)	Hydrophone Depth (m)	Instrument Type	Sampling Frequency (kHz)	Sensitivity (dB re 1 V/μPa)
CBN	47.1619	-60.3931	148	AMAR G4	32	-153.0
CSW	47.3789	-60.2991	115	AMAR M20	n/a	n/a
CS1	47.4345	-60.0532	443	AMAR G4-UD	128	-165.116
CS2	43.4973	-62.8699	487	AMAR G4-UD	128	-165.216
CS3	44.6925	-66.5311	457	AMAR G4-UD	128	-164.716
CSE	44.6916	-66.5299	154	ST600 (SN6767)	48	-175.7
CSE	44.6916	-66.5299	154	ST600 (SN6769)	48	-175.8

7 FIGURES

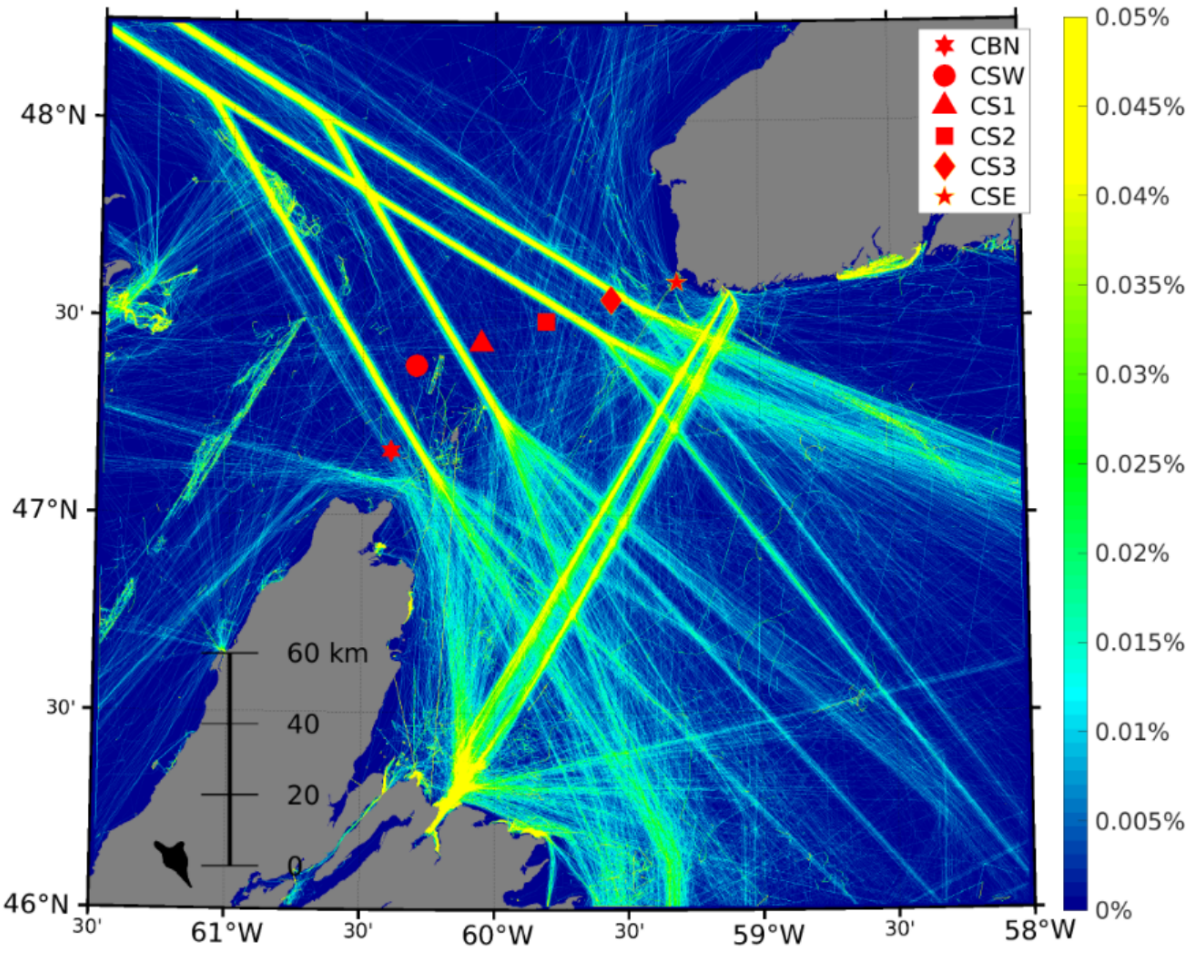

Figure 1. Mooring stations: Cape Breton North (CBN), Cabot Strait West (CSW), Cabot Strait 1 (CS1), Cabot Strait 2 (CS2), Cabot Strait 3 (CS3), and Cabot Strait East (CSE), overlaid on a vessel density map. Vessel density is in the unit of percent of time per square km for the period of Jan 1 2022 to Dec 31, 2022.

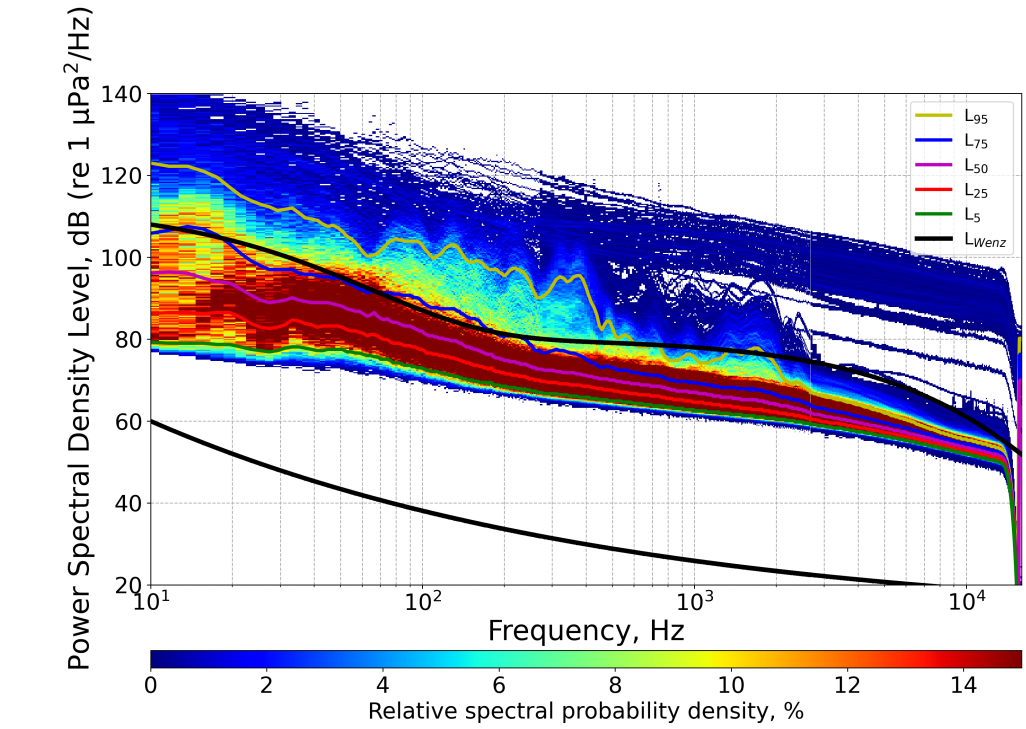

(a)

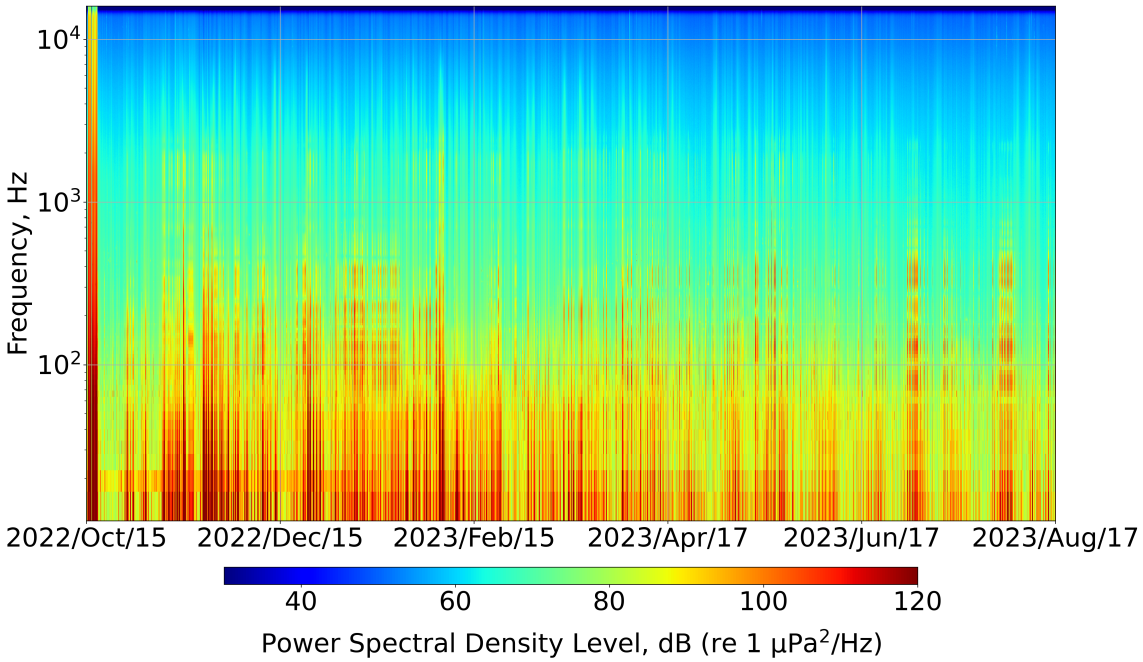

(b)

Figure 2. Relative spectral probability density (RSPD) (a), the black lines represent the upper and lower limits of the Wenz Spectrum, and the yellow, blue, magenta, red, and green lines correspond to the 95th, 75th, 50th, 25th, and 5th percentile power spectra, respectively; and Spectrogram (b) of CBN Channel 4.

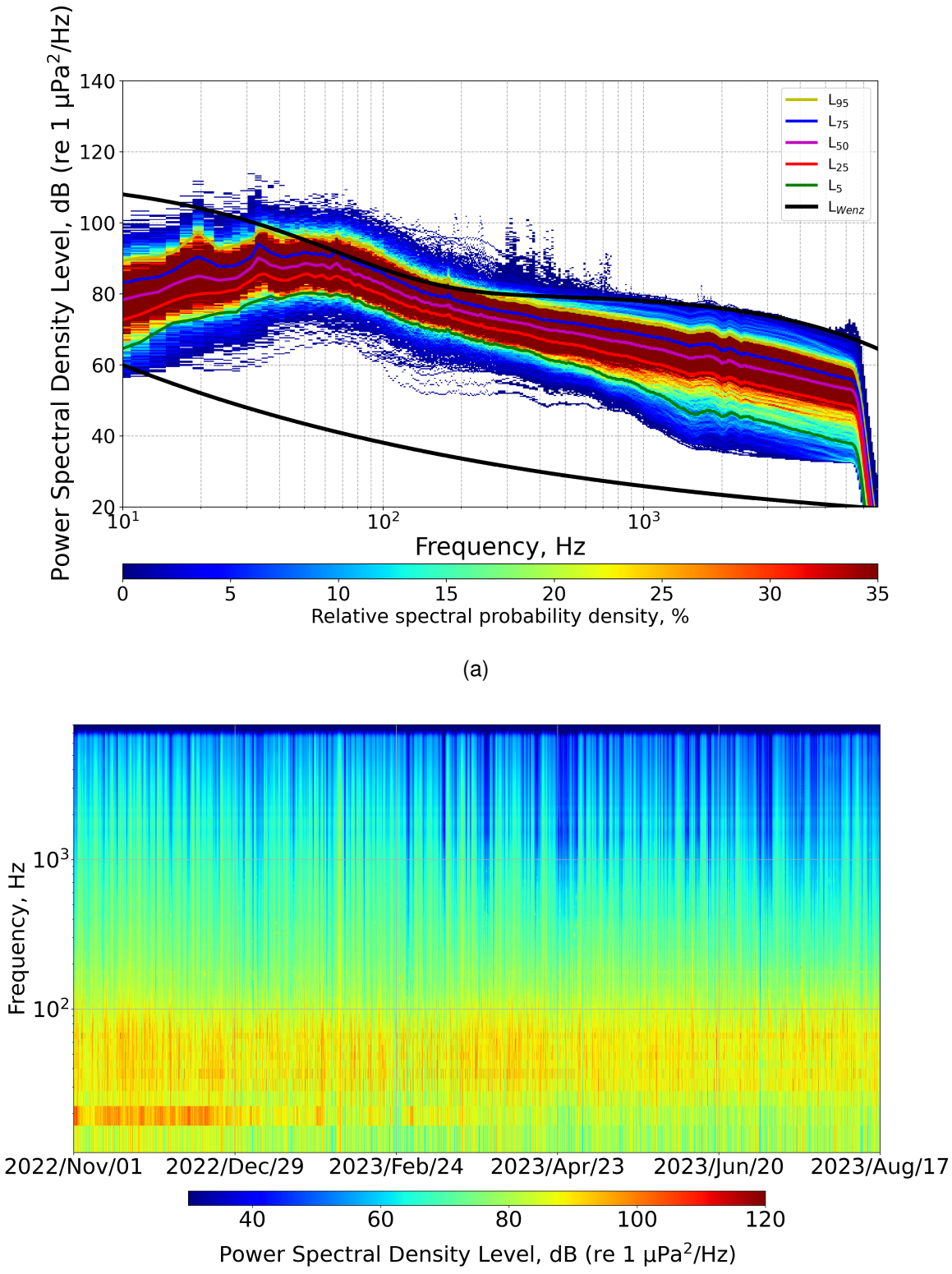

Figure 3. Relative spectral probability density (RSPD) (a), the black lines represent the upper and lower limits of the Wenz Spectrum, and the yellow, blue, magenta, red, and green lines correspond to the 95th, 75th, 50th, 25th, and 5th percentile power spectra, respectively; and Spectrogram (b) of CS1.

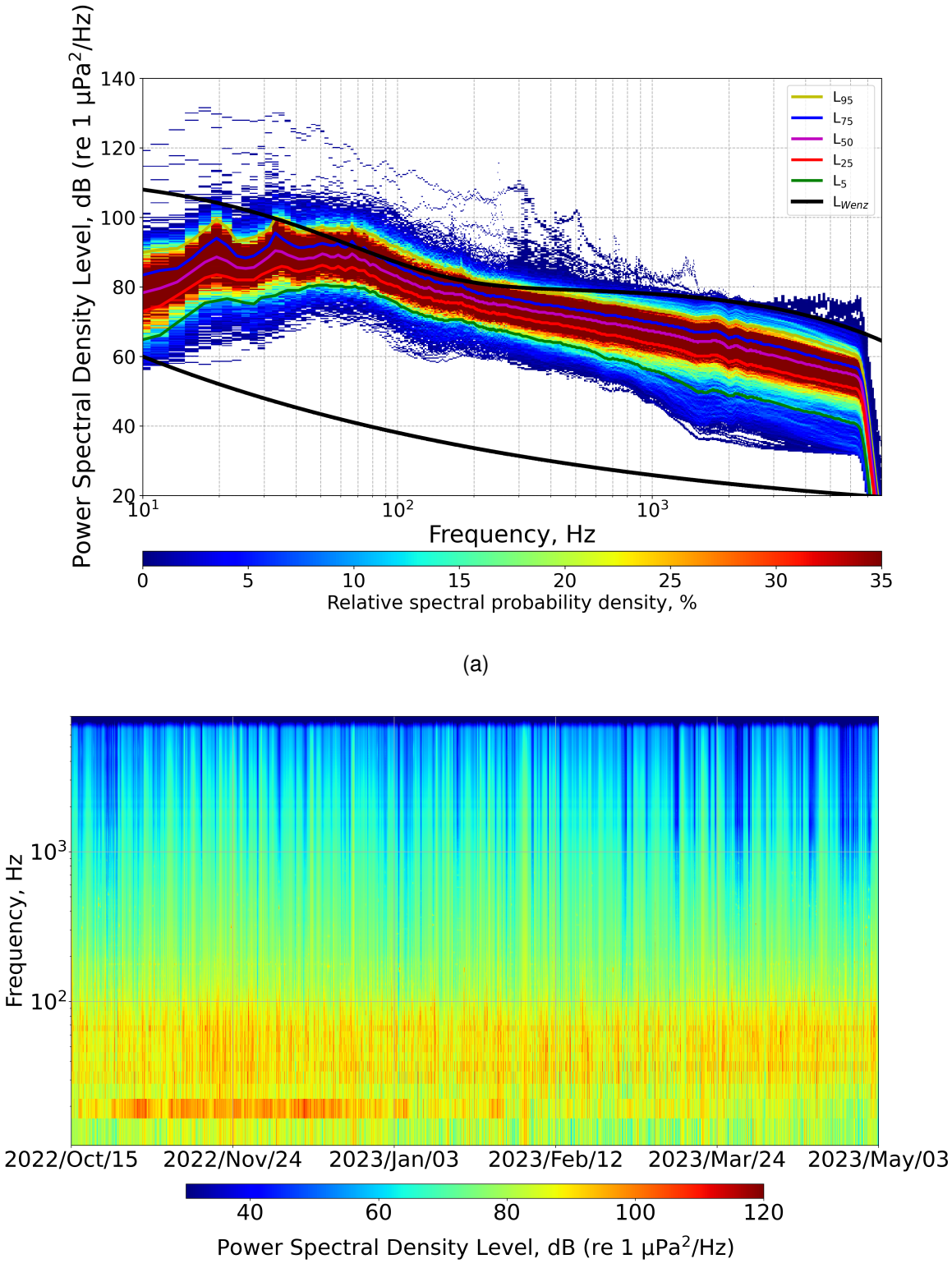

Figure 4. Relative spectral probability density (RSPD) (a), the black lines represent the upper and lower limits of the Wenz Spectrum, and the yellow, blue, magenta, red, and green lines correspond to the 95th, 75th, 50th, 25th, and 5th percentile power spectra, respectively; and Spectrogram (b) of CS2.

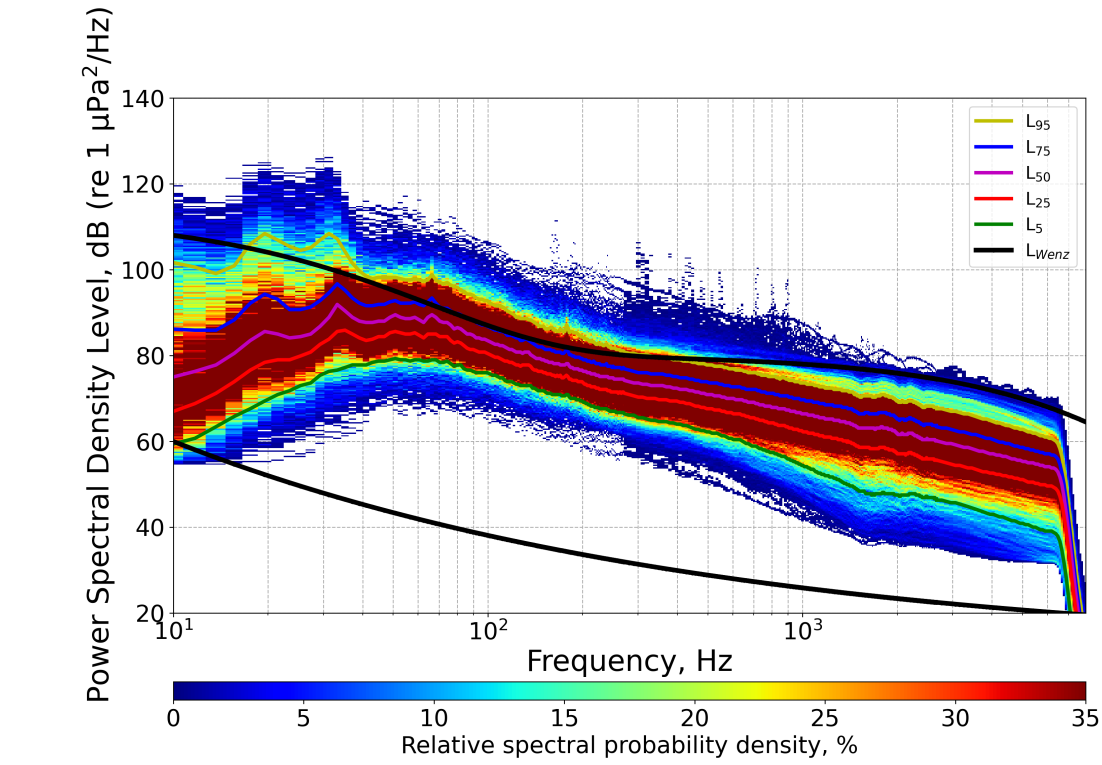

(a)

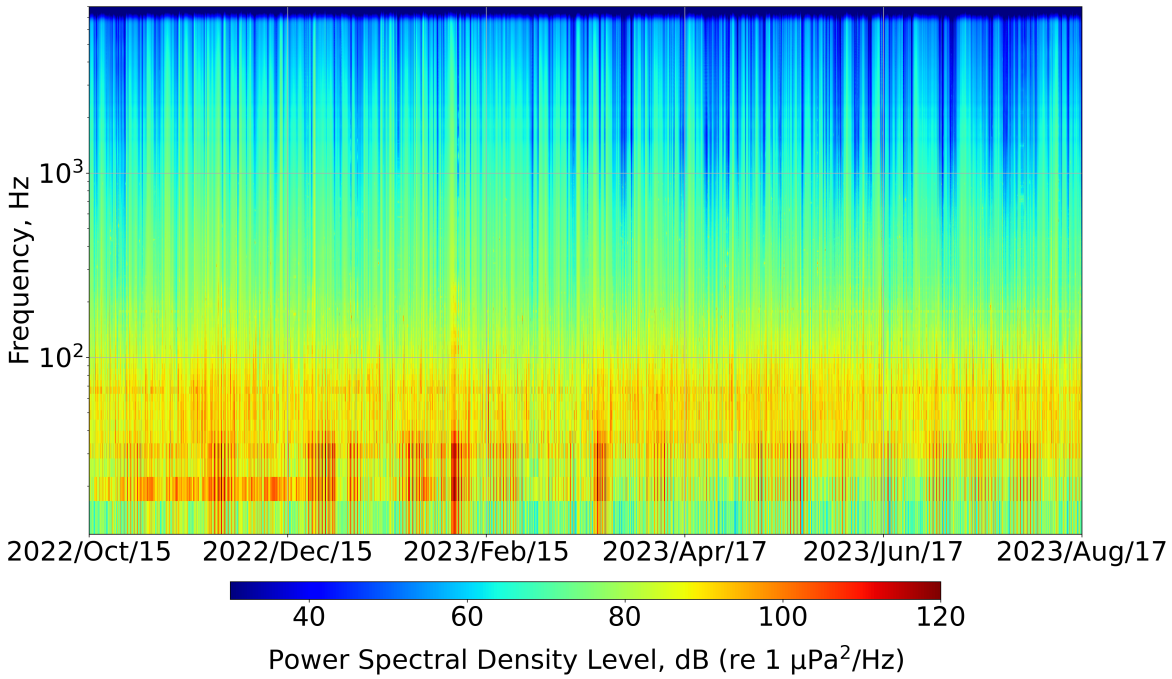

(b)

Figure 5. Relative spectral probability density (RSPD) (a), the black lines represent the upper and lower limits of the Wenz Spectrum, and the yellow, blue, magenta, red, and green lines correspond to the 95th, 75th, 50th, 25th, and 5th percentile power spectra, respectively; and Spectrogram (b) of CS3.

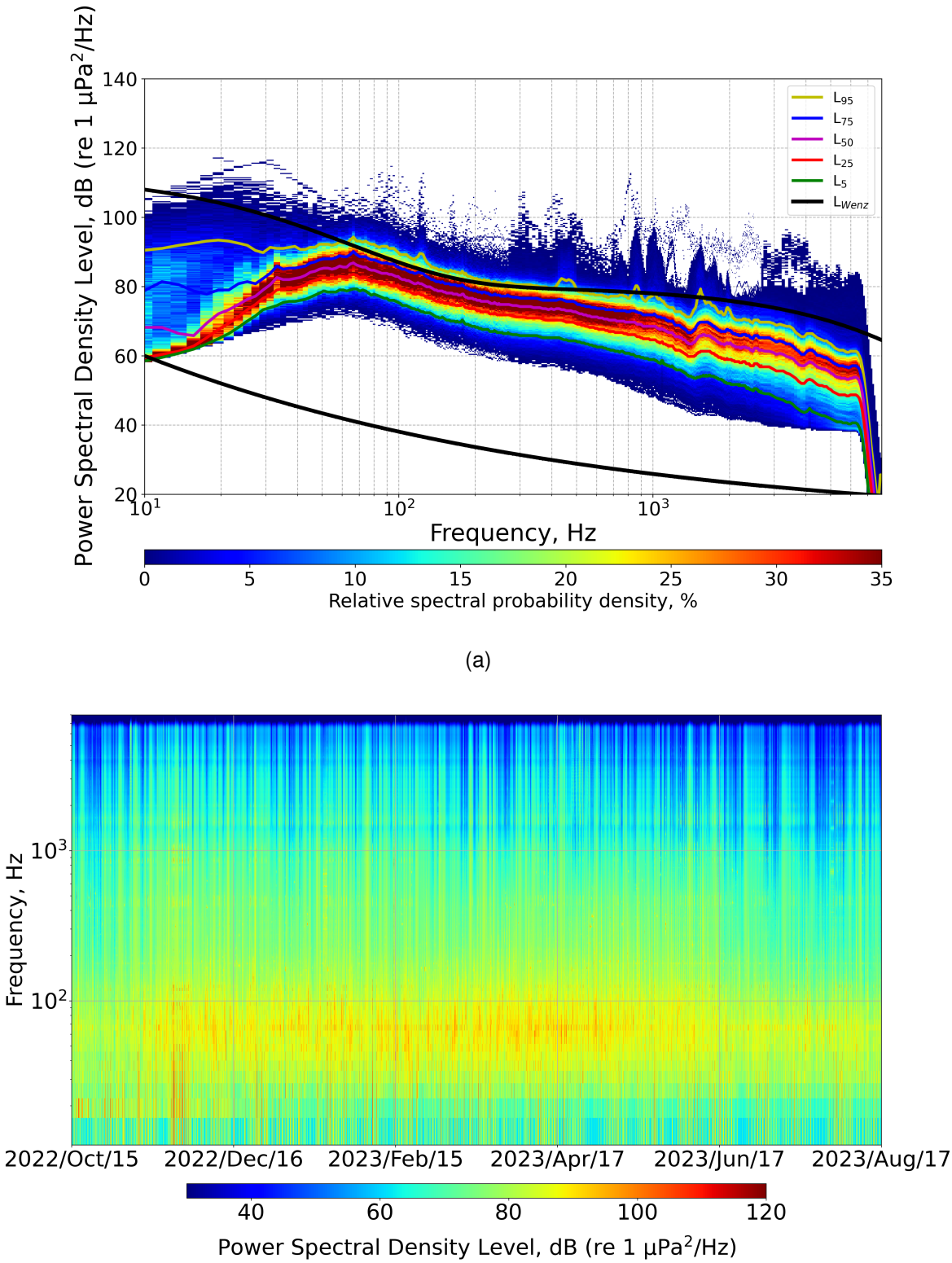

Figure 6. Relative spectral probability density (RSPD) (a), the black lines represent the upper and lower limits of the Wenz Spectrum, and the yellow, blue, magenta, red, and green lines correspond to the 95th, 75th, 50th, 25th, and 5th percentile power spectra, respectively; and Spectrogram (b) of CSE (SN6767)(Table 2).

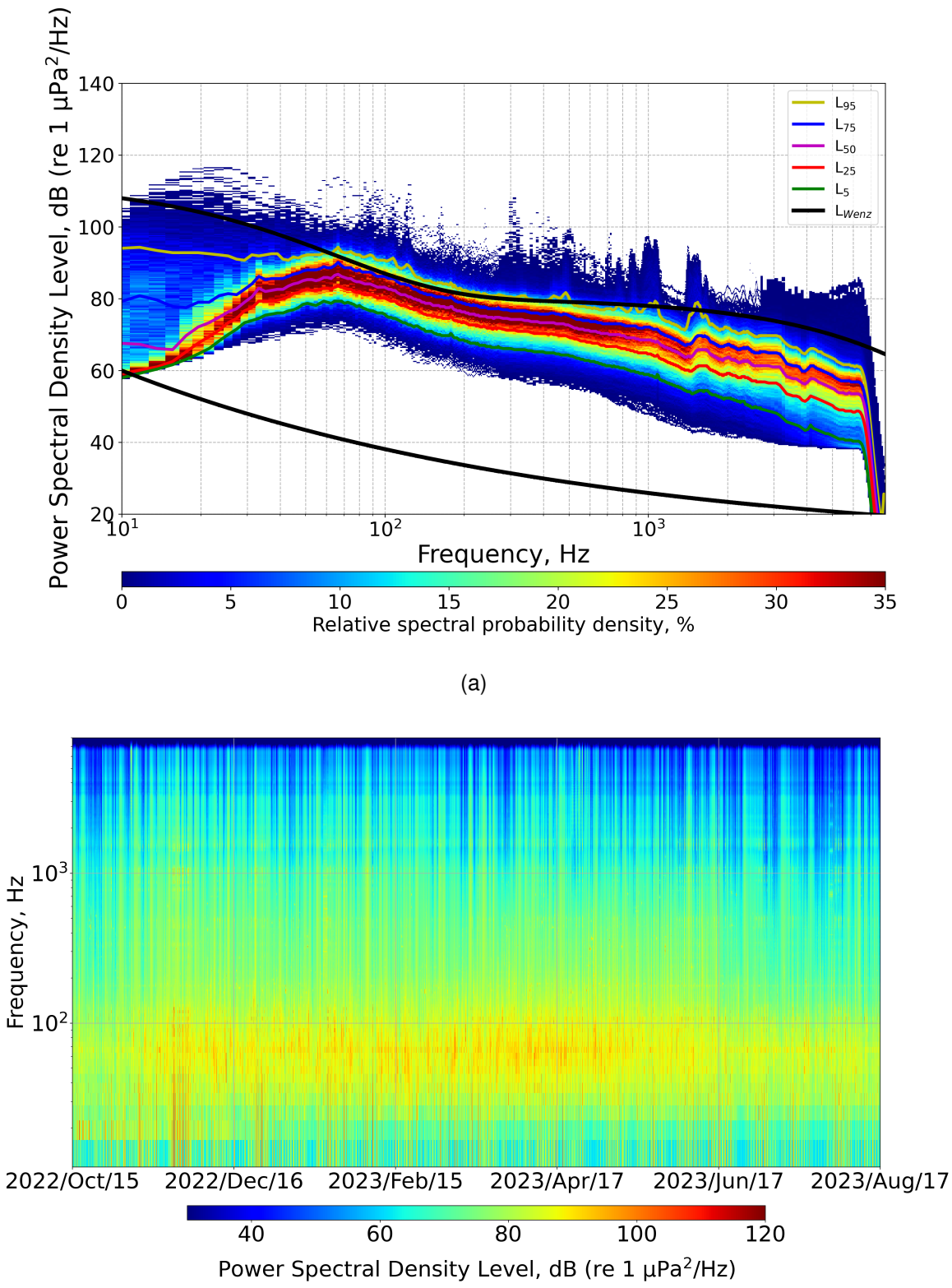

Figure 7. Relative spectral probability density (RSPD) (a), the black lines represent the upper and lower limits of the Wenz Spectrum, and the yellow, blue, magenta, red, and green lines correspond to the 95th, 75th, 50th, 25th, and 5th percentile power spectra, respectively; and Spectrogram (b) of CSE (SN6769)(Table 2).

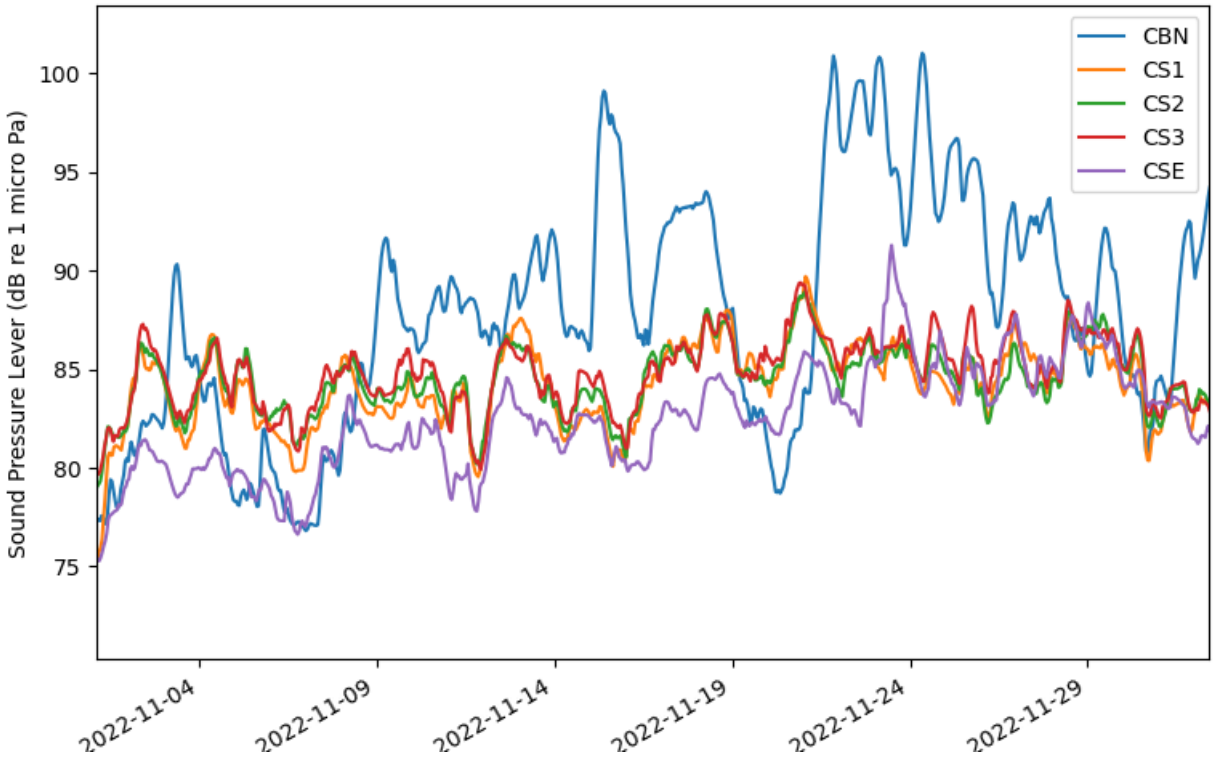

Figure 8. November 2022 1/3 octave band (80 - 105 Hz) sound pressure level for the five mooring stations: CBN, CS1, CS2, CS3, and CSE.

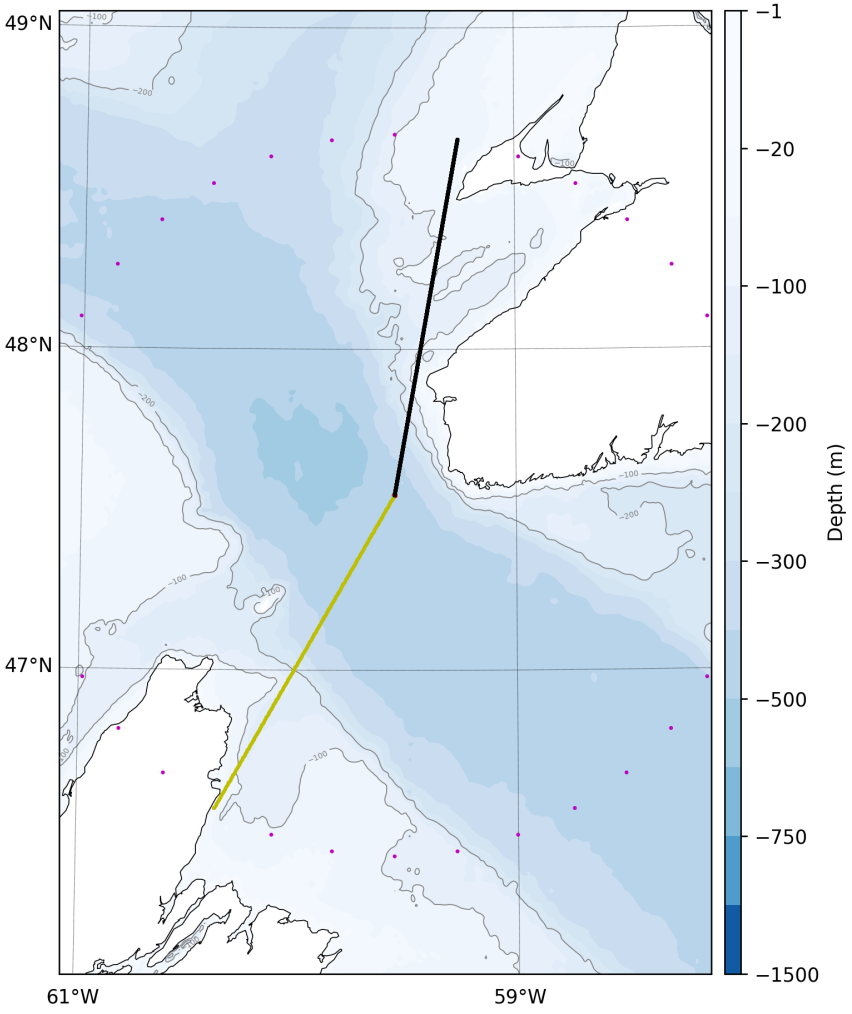

(a)

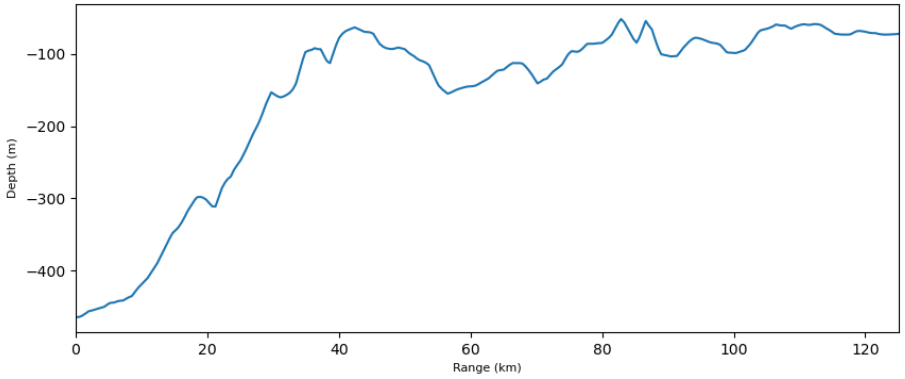

(b)

Figure 9. Nx2D sound propagation setup and bathymetry. (a) A top-view sound propagation path with radius of 120 km from station CS3 where magenta points indicate the various azimuthal directions used for Nx2D simulations; (b) bottom profiles of sound propagation for station CS3 at an azimuth of 10 degrees relative to due north.

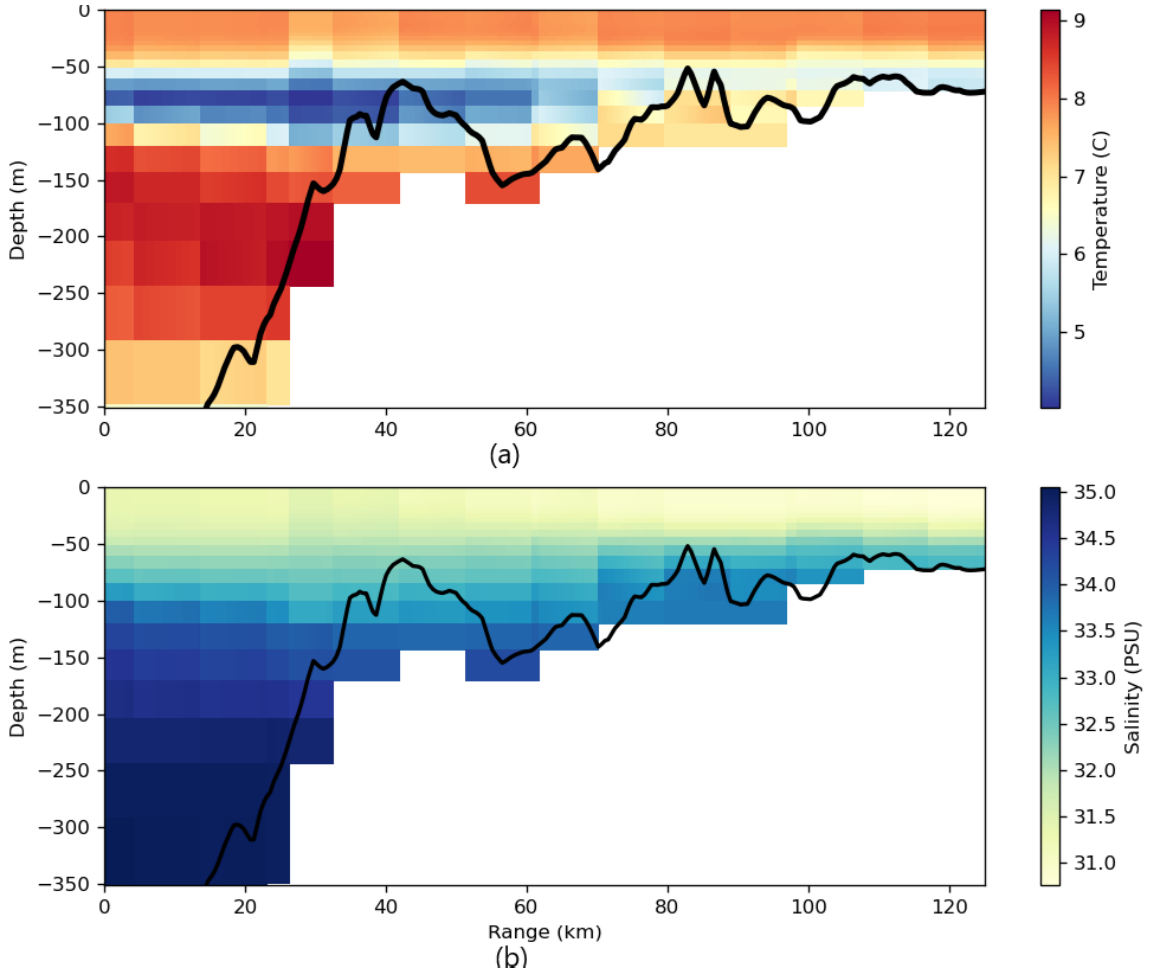

Figure 10. The temperature (a) and salinity (b) fields extracted from the GLORYS reanalysis dataset for CS3 at an azimuth of 10 degrees relative to due north. The black lines indicate the bottom profiles from bathymetry dataset.

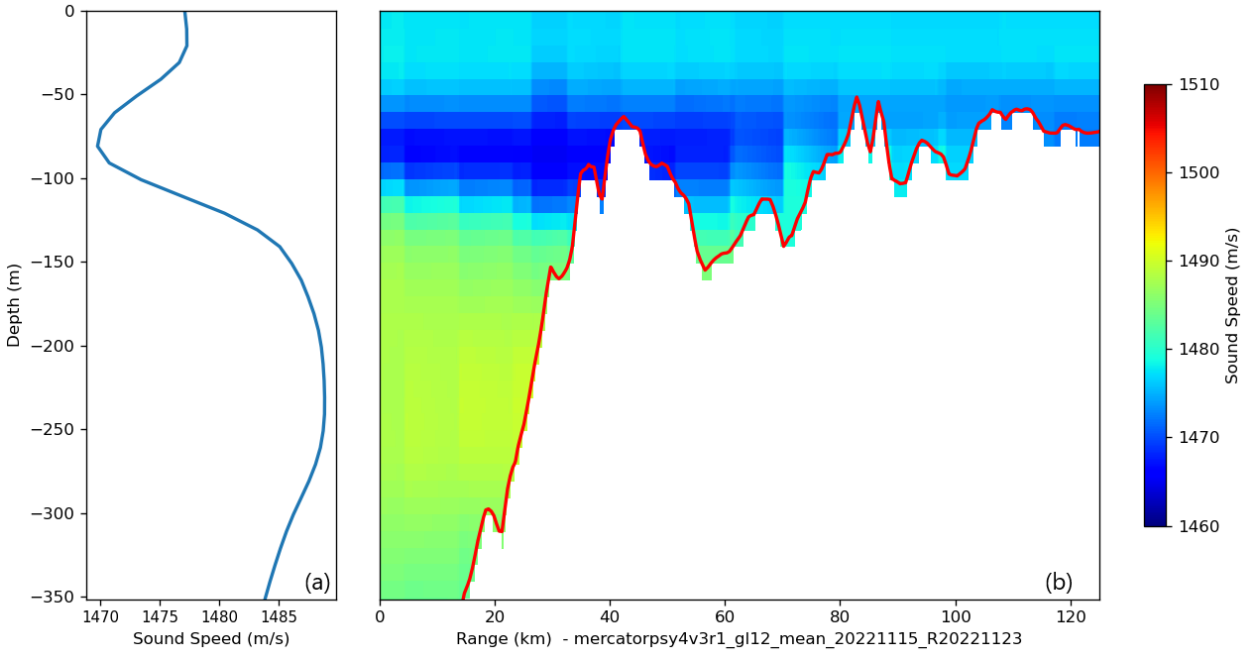

Figure 11. The sound speed field constructed from the GLORYS temperature and salinity data for CS3 at an azimuth of 10 degrees relative to due north: (a) the range averaged sound speed profile and (b) range dependent sound speed field.

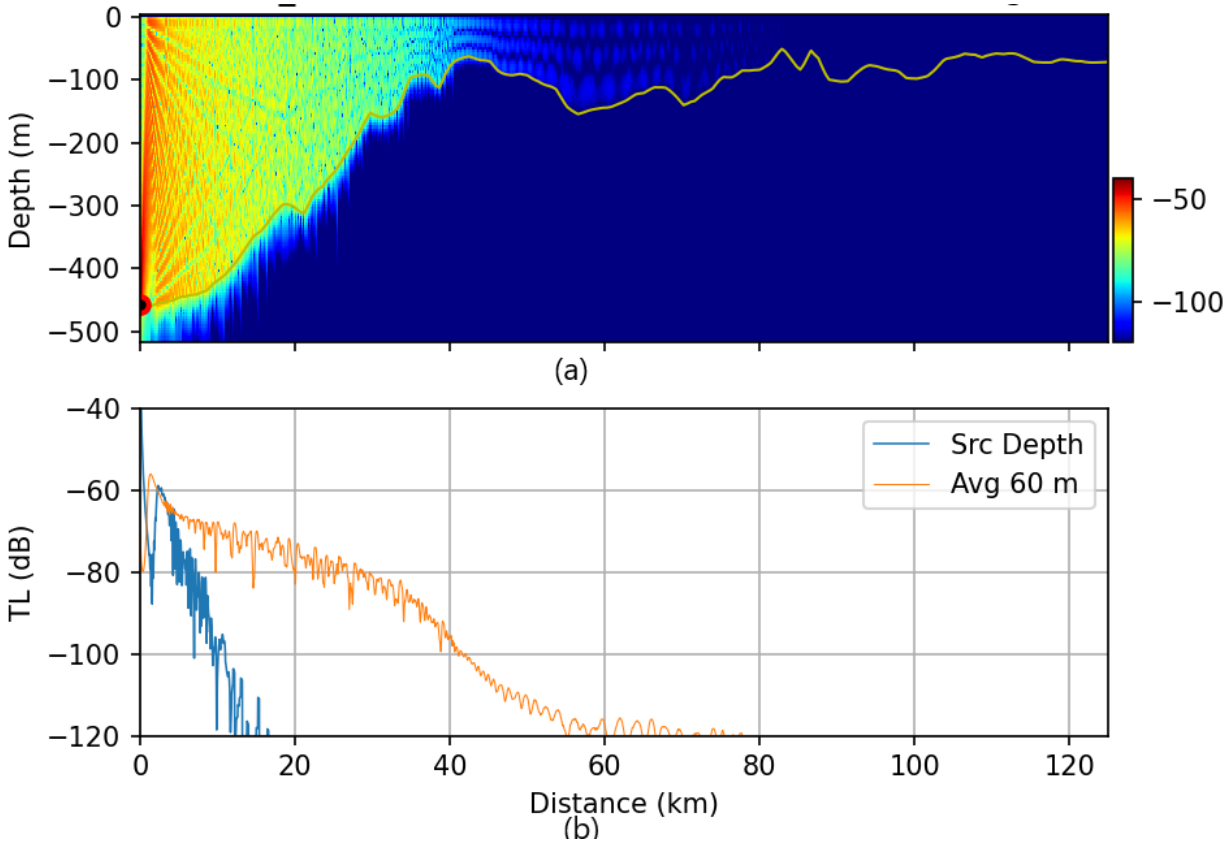

Figure 12. Transmission loss for a 100 Hz sound source at CS3, at an azimuth of 10 degrees relative to due North: (a) the full field transmission loss; (b) the average transmission loss as function of distance of first 60 m depth average (orange line) and the transmission loss at depth of mooring location (blue line).

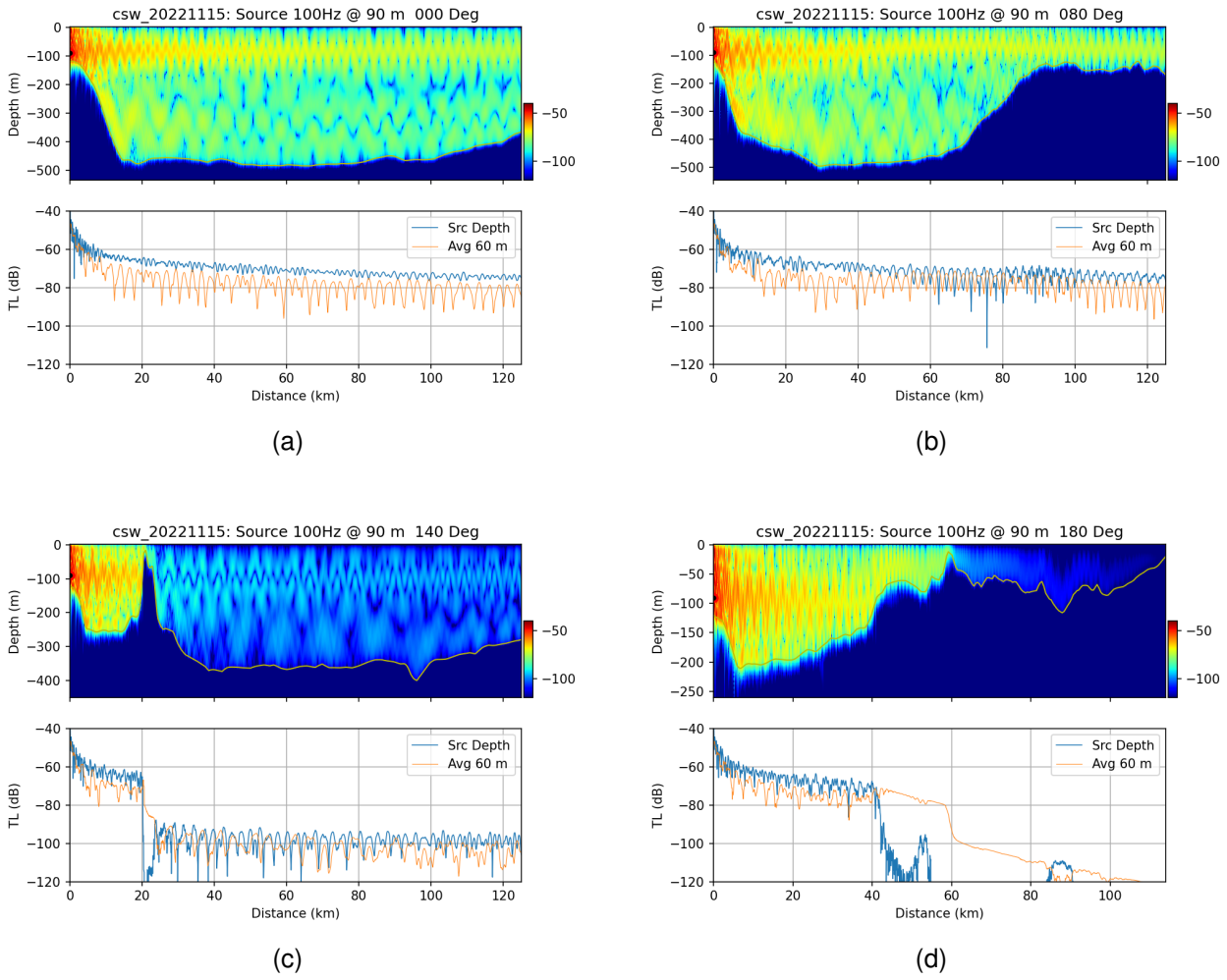

Figure 13. Nx2D sound propagation modelling for CSW for four different directions: (a) CSW 0 degree w.r.t. due north; (b) CSW 80 degree w.r.t. due north; (c) CSW 140 degree w.r.t. due north; (d) CSW 180 degree w.r.t. due north.

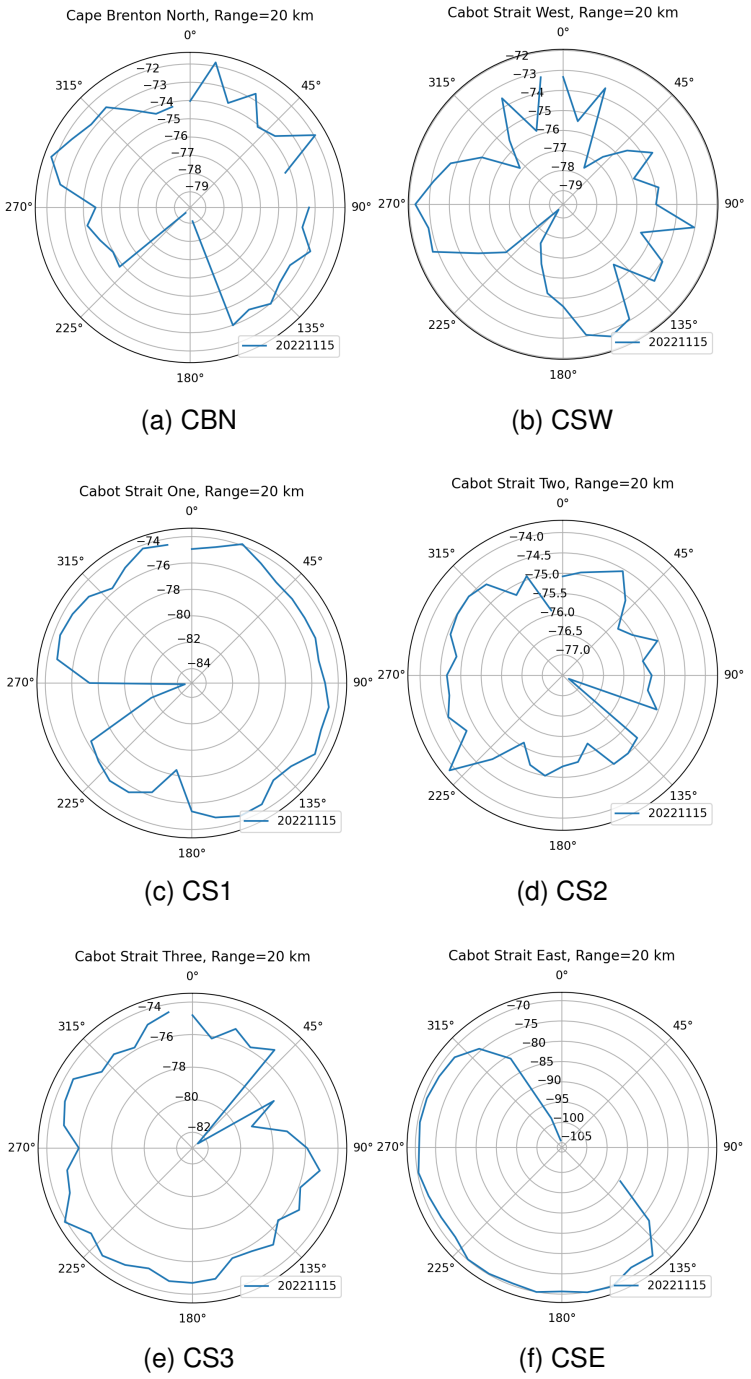

(a) CBN (b) CSW

(c) CS1 (d) CS2

(e) CS3 (f) CSE

Figure 14. Polar plot representing averaged transmission loss (dB) within the first 60 meters of water depth at a 20 km distance from the sound source estimated using Nx2D modeling for all stations on November 15, 2022. The concentric circles indicate transmission loss in decibels (dB), with each ring corresponding to a specific loss value labeled on the plot. Radial lines represent azimuthal directions (degrees), where 0° points north. Note that the center of the plot corresponds to the highest transmission loss (i.e., greatest acoustic attenuation), while points farther from the center have lower transmission loss. This presentation emphasizes the directional variability in acoustic propagation conditions at the different stations.

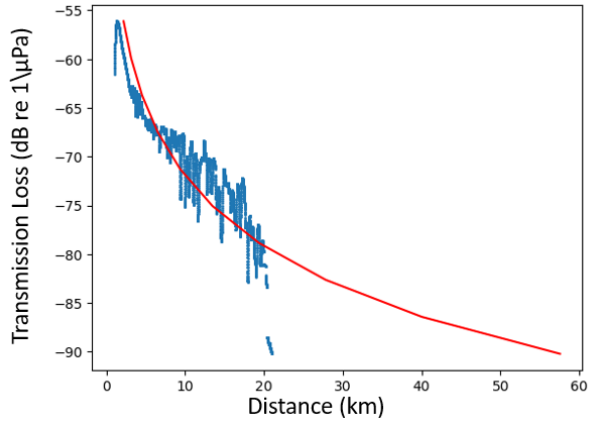

(a)

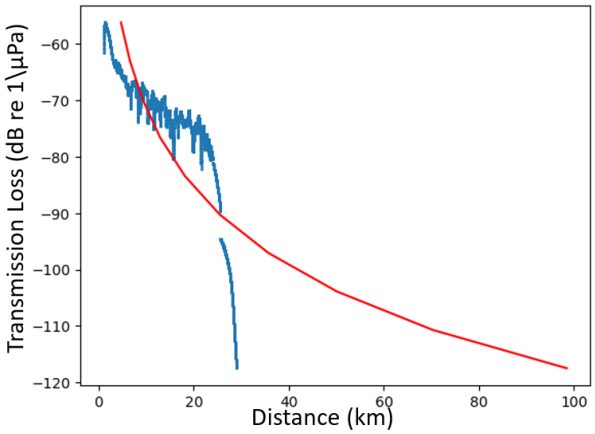

(b)

Figure 15. Transmission Loss (TL) as a function of range with a logarithmic regression fit: (a) shows TL as a function of range for CS3 at an azimuth of 60 degrees relative to due north;(b) represents the azimuth of 40 degrees relative to due north. The blue line represents transmission loss as function of range based on acoustic propagation modeling, while the red line depicts the logarithmic regression model.

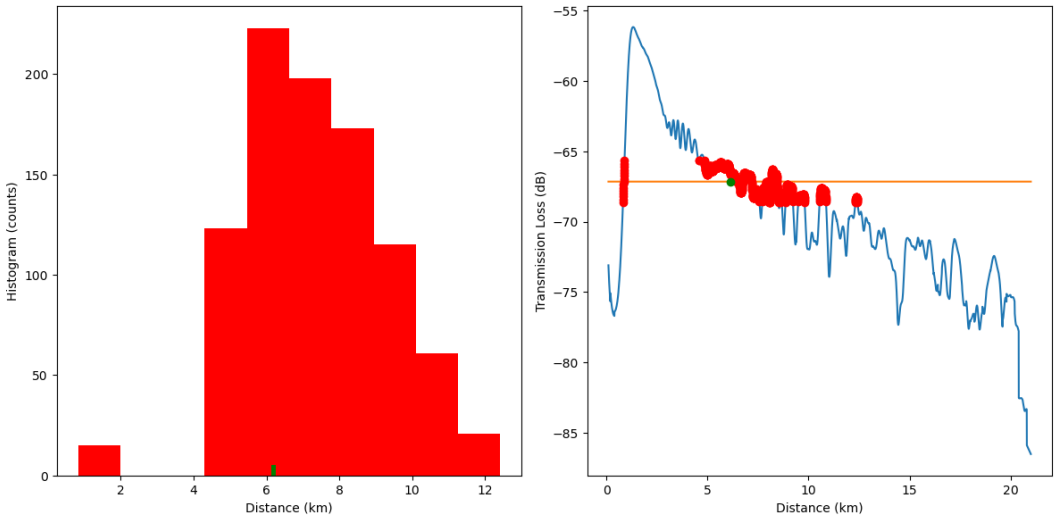

(a) TL vs range for CS3 at an azimuth of 60 degrees relative to due north.

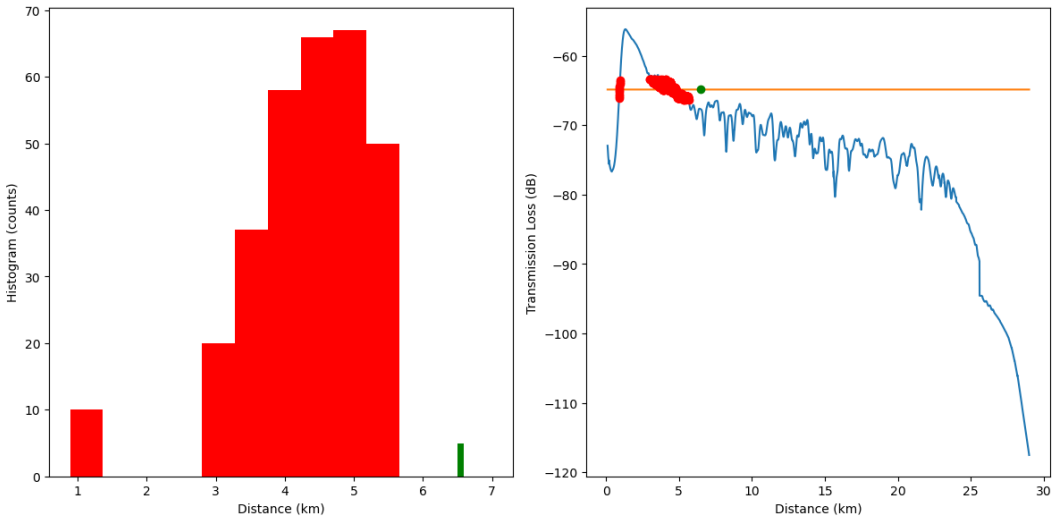

(b) TL vs range for CS3 at an azimuth of 40 degrees relative to due north.

Figure 16. Two examples of quantile regression compared to logarithmic regression in transmission loss (TL) as a function of range, with a logarithmic regression fit shown in the two right-hand panels. The upper panels show results for CS3 at an azimuth of 60 degrees relative to due north, while the lower panels display results for CS3 at an azimuth of 40 degrees relative to due north. In each case, the blue line indicates transmission loss as a function of range based on acoustic propagation modeling. The horizontal orange lines represent the value of TL_{det} as defined in Eq. 7. Green markers (dots in the right column and bars in the left column) indicate the solution based on the logarithmic regression model. Red markers in the right panels and histograms in the left panels represent distances obtained from propagation modeling, corresponding to transmission loss values within $\pm 1.5dB$ of TL_{det}.

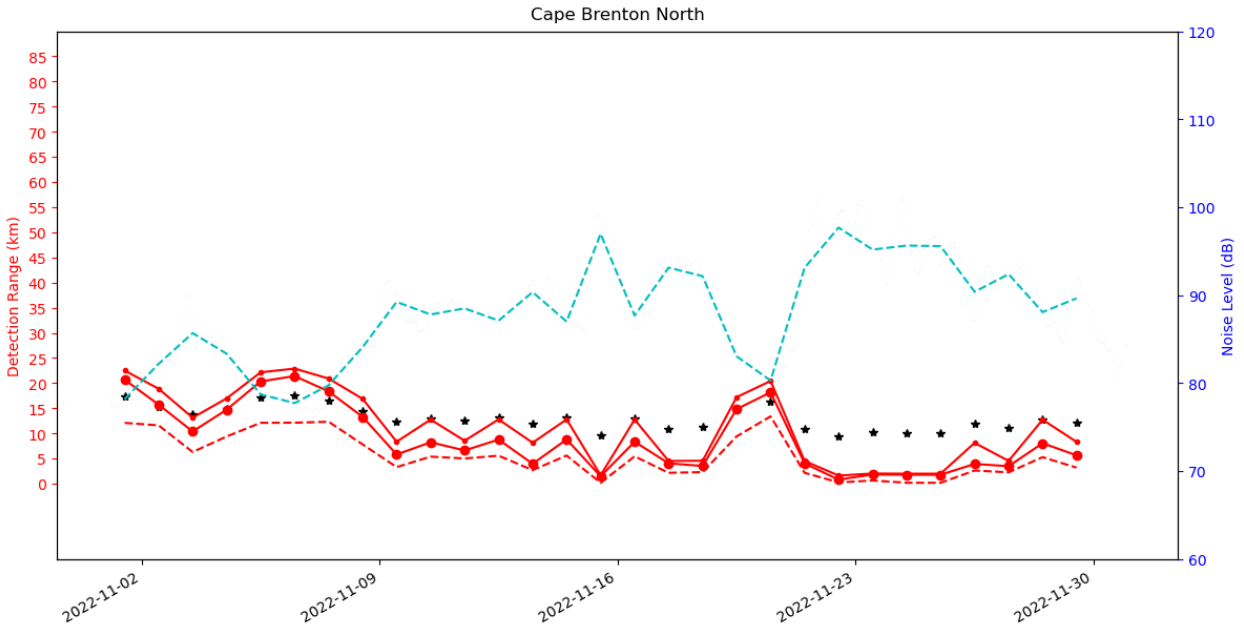

Figure 17. CBN Station: Detection distance estimation and background noise level for November 2022 at an azimuth of 320 degrees relative to due north. The light blue dashed line represents the daily average noise level. The red lines indicate the detection distance based on the quantile regression model, where the solid, dotted, and dashed red lines correspond to the 95th, 50th (median), and 5th percentiles, respectively. The black stars denote detection distances estimated using the logarithmic regression model.

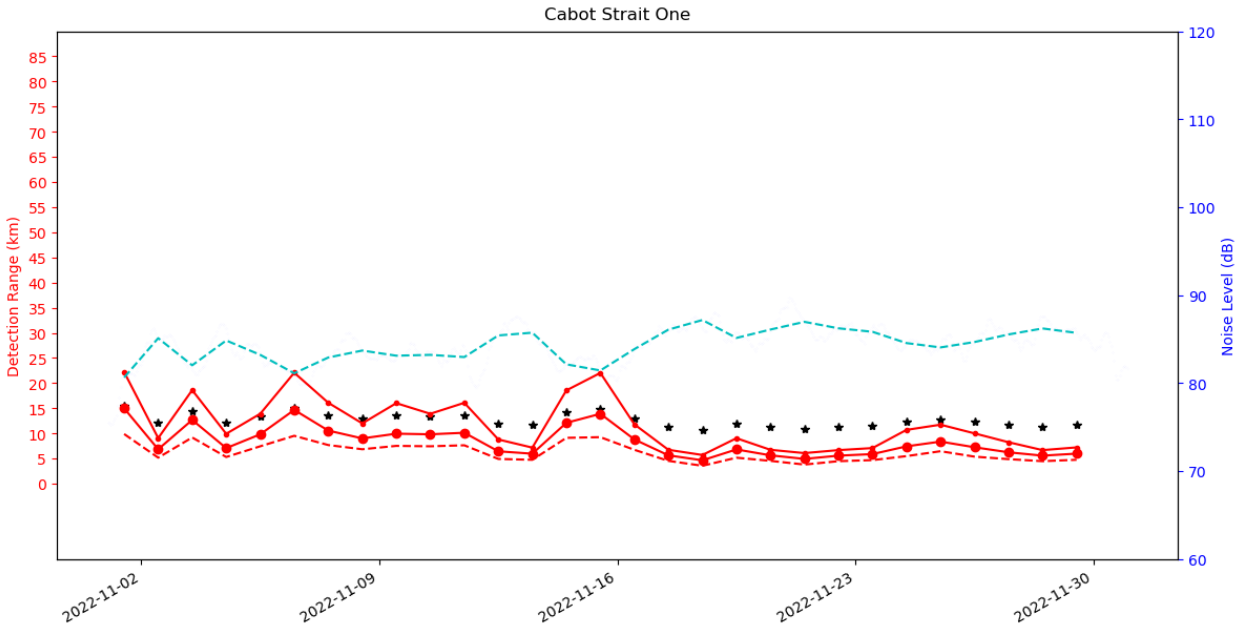

Figure 18. CS1 Station: Detection distance estimation and background noise level for November 2022 at an azimuth of 310 degrees relative to due north. The light blue dashed line represents the daily average noise level. The red lines indicate the detection distance based on the quantile regression model, where the solid, dotted, and dashed red lines correspond to the 95th, 50th (median), and 5th percentiles, respectively. The black stars denote detection distances estimated using the logarithmic regression model.

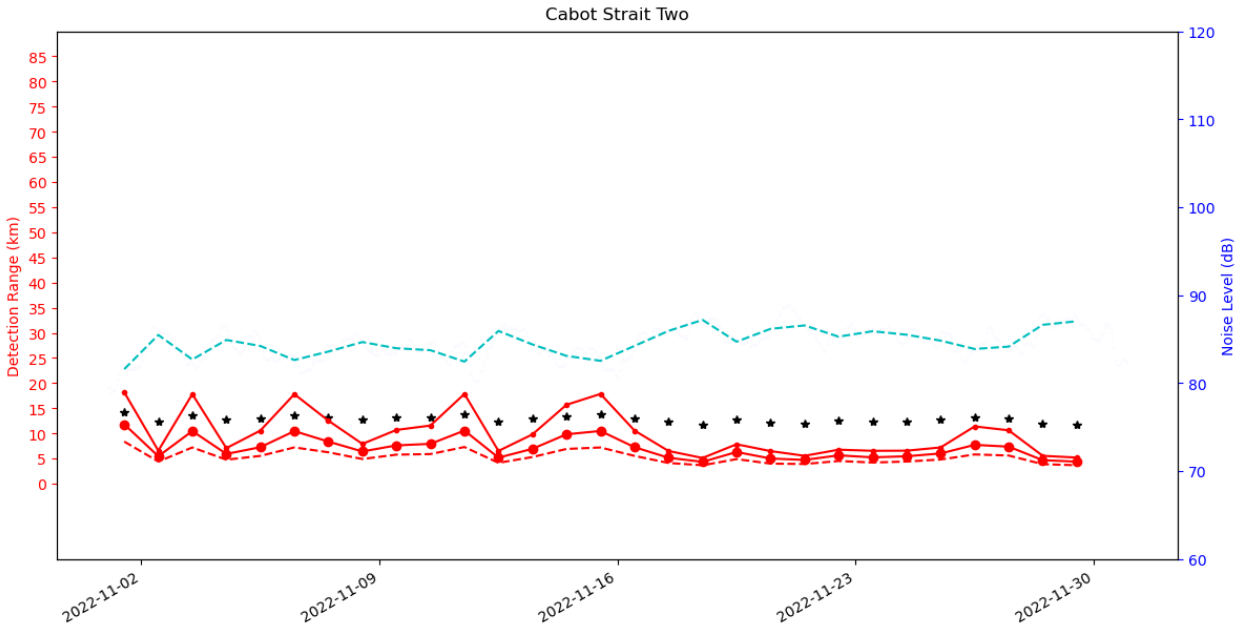

Figure 19. CS2 Station: Detection distance estimation and background noise level for November 2022 at an azimuth of 250 degrees relative to due north. The light blue dashed line represents the daily average noise level. The red lines indicate the detection distance based on the quantile regression model, where the solid, dotted, and dashed red lines correspond to the 95th, 50th (median), and 5th percentiles, respectively. The black stars denote detection distances estimated using the logarithmic regression model.

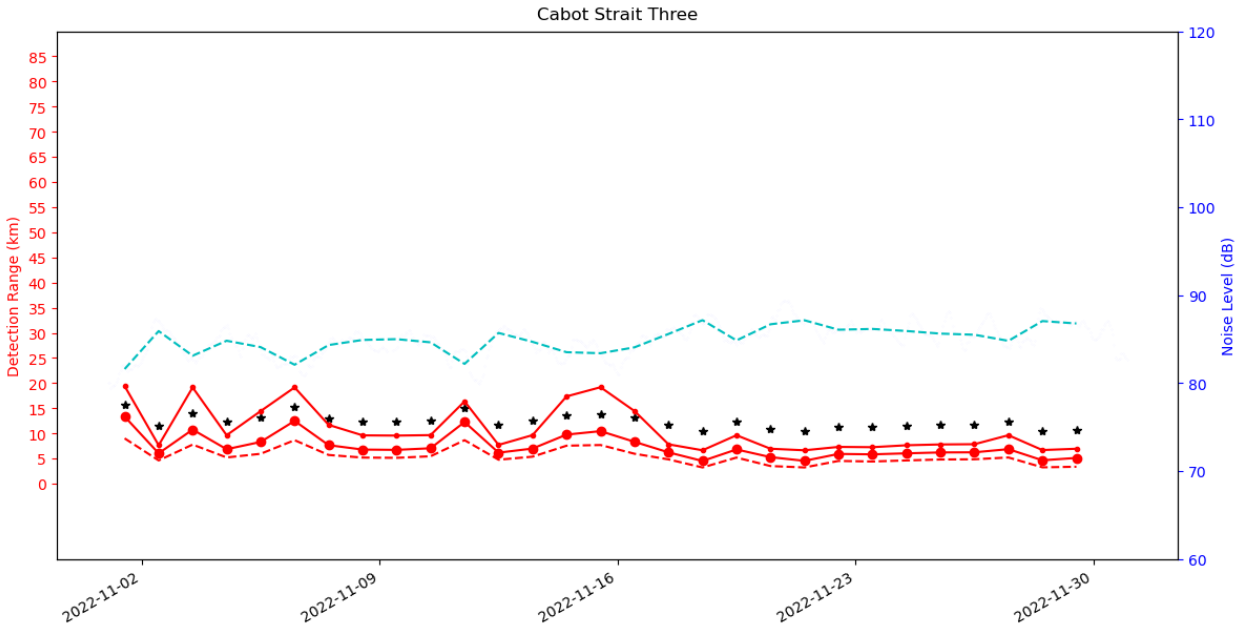

Figure 20. CS3 Station: Detection distance estimation and background noise level for November 2022 at an azimuth of 220 degrees relative to due north. The light blue dashed line represents the daily average noise level. The red lines indicate the detection distance based on the quantile regression model, where the solid, dotted, and dashed red lines correspond to the 95th, 50th (median), and 5th percentiles, respectively. The black stars denote detection distances estimated using the logarithmic regression model.

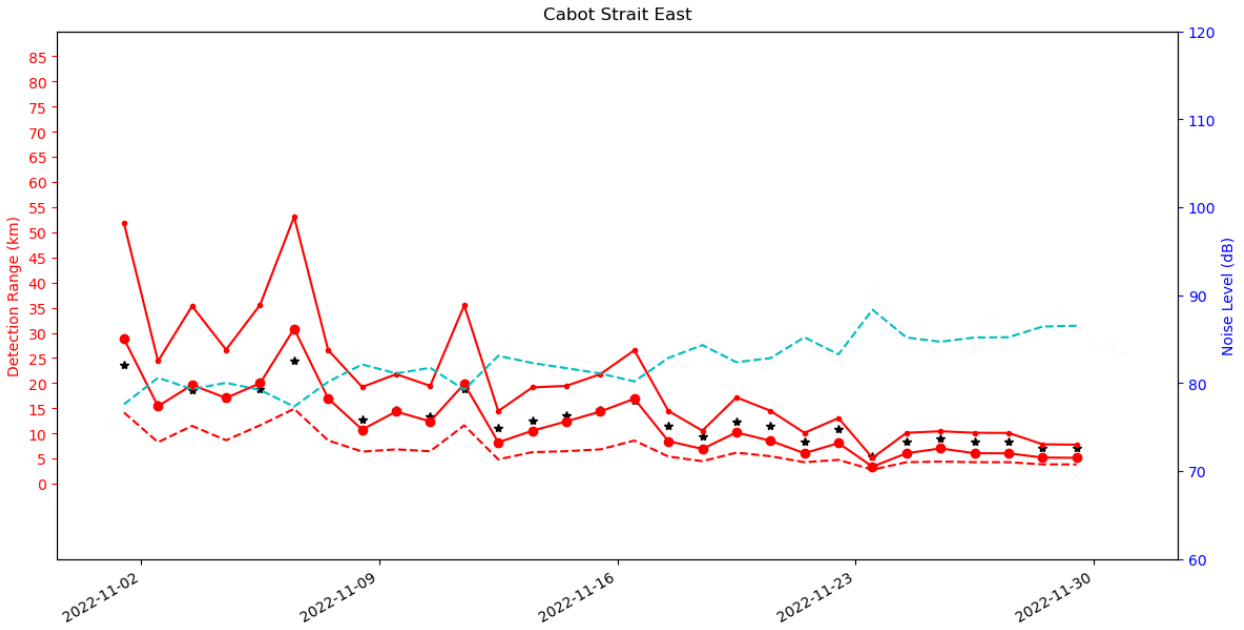

Figure 21. CSE Station: Detection distance estimation and background noise level for November 2022 at an azimuth of 320 degrees relative to due north. The light blue dashed line represents the daily average noise level. The red lines indicate the detection distance based on the quantile regression model, where the solid, dotted, and dashed red lines correspond to the 95th, 50th (median), and 5th percentiles, respectively. The black stars denote detection distances estimated using the logarithmic regression model.

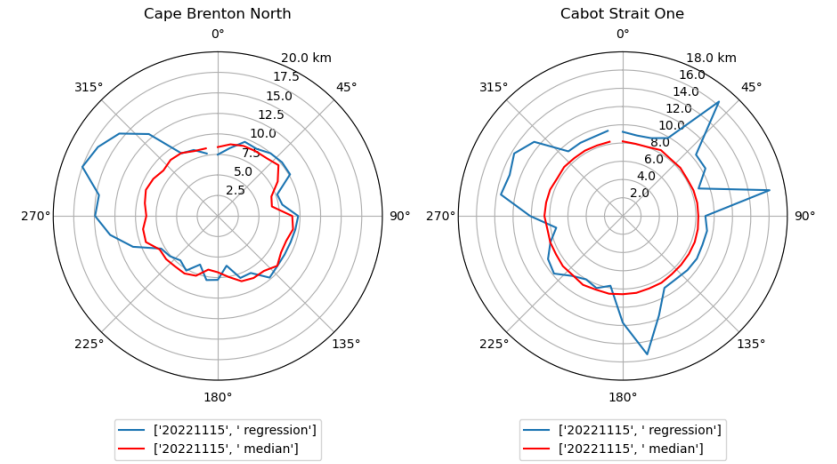

(a) CBN

(b) CS1

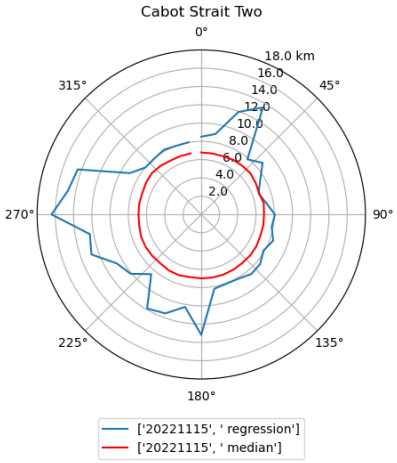

(c) CS2

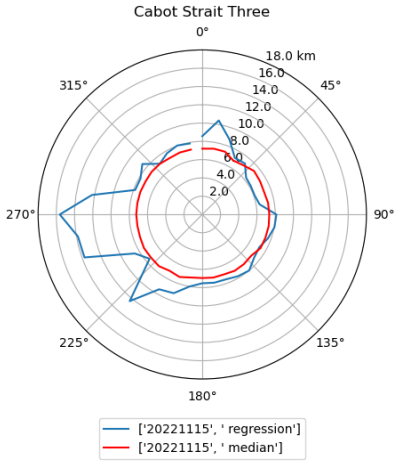

(d) CS3

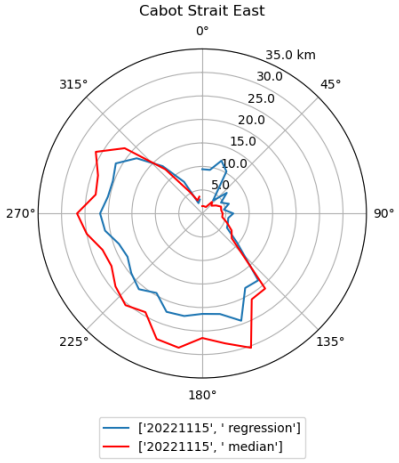

(e) CSE

Figure 22. Monthly averaged detection range estimation for all stations with available measurements in November 2022. The blue line represents the results using the logarithmic regression model, while the red line represents the modified quantile regression model.

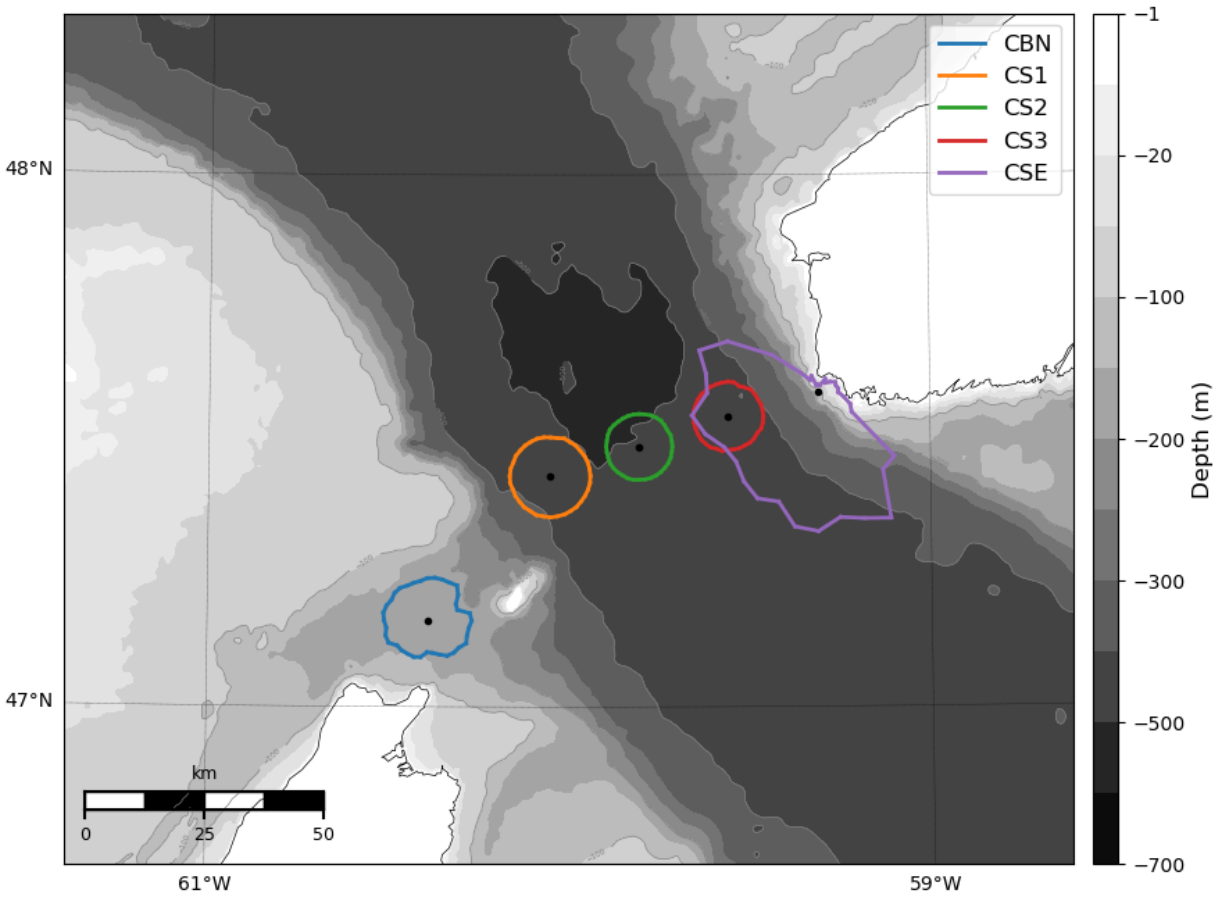

Figure 23. Top view of detection ranges result for November 2022 for five stations.

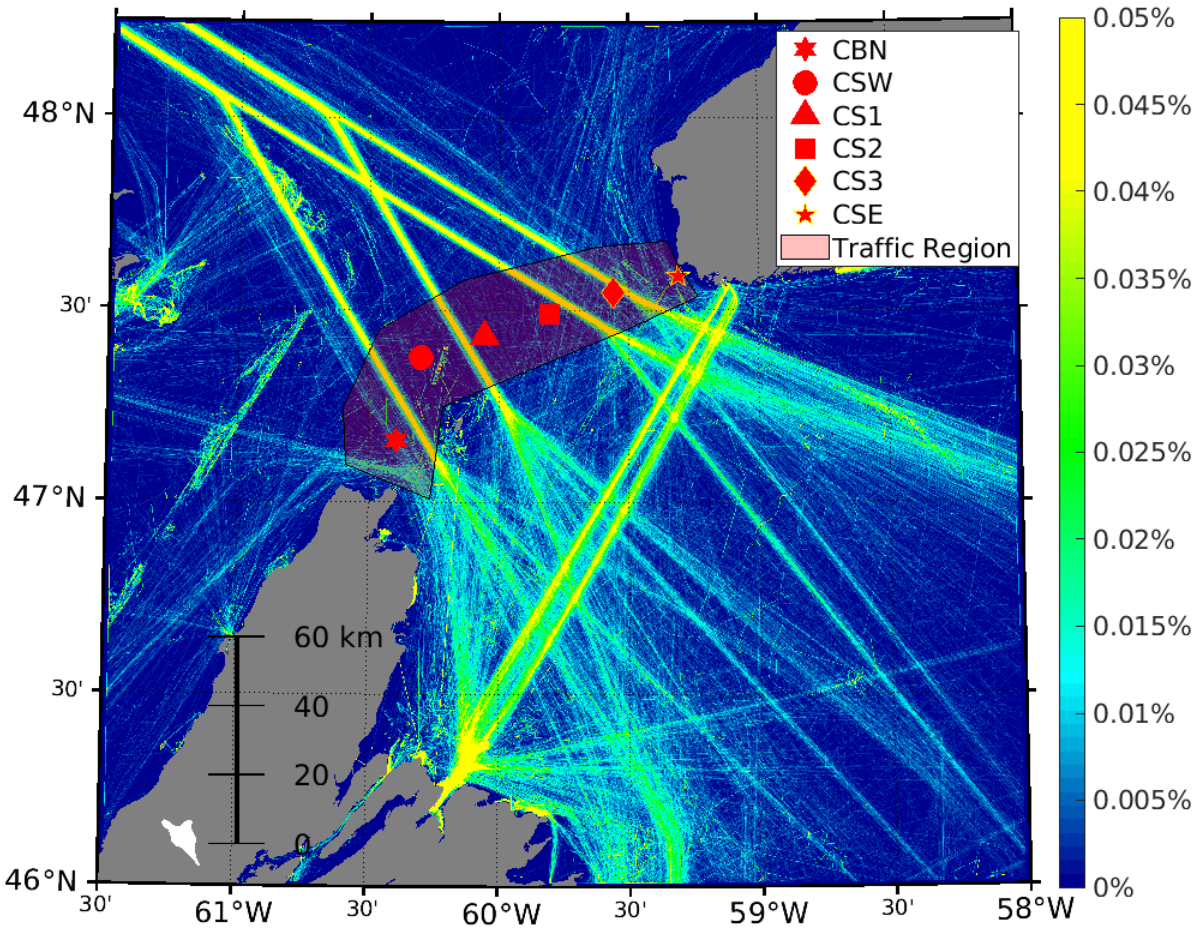

Figure 24. Mooring locations overlaid on a vessel density map. The red frame highlights the region where vessel data were analyzed as part of this study, including vessel types and numbers.

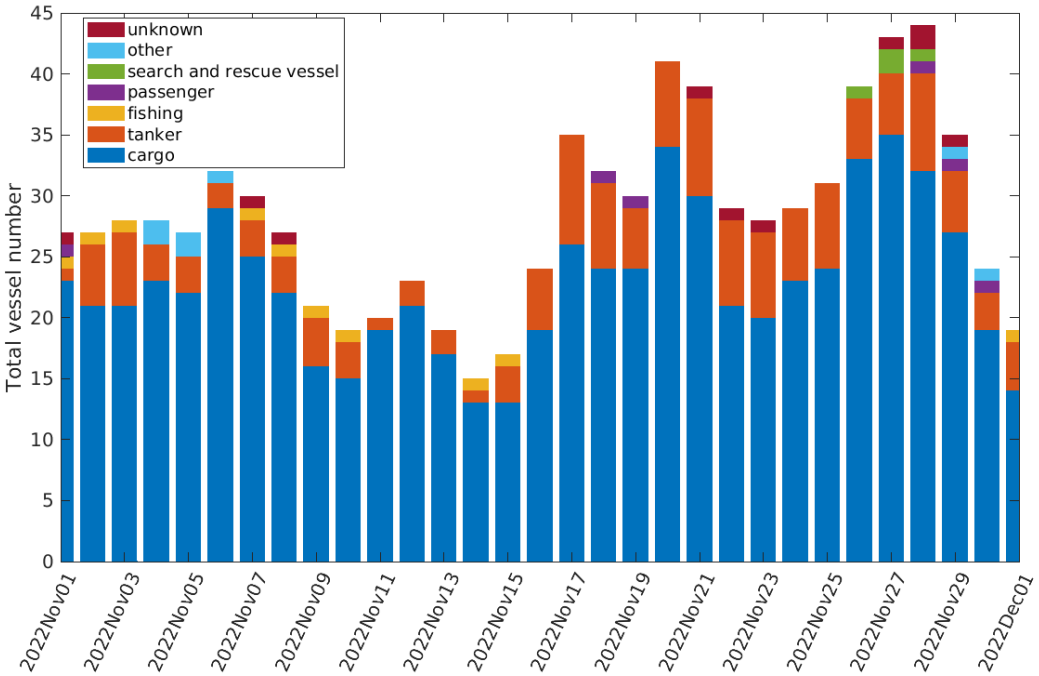

Figure 25. Daily statistics of vessel types and numbers in the vicinity of the Cabot Strait moorings from November 1 to November 30 2022.

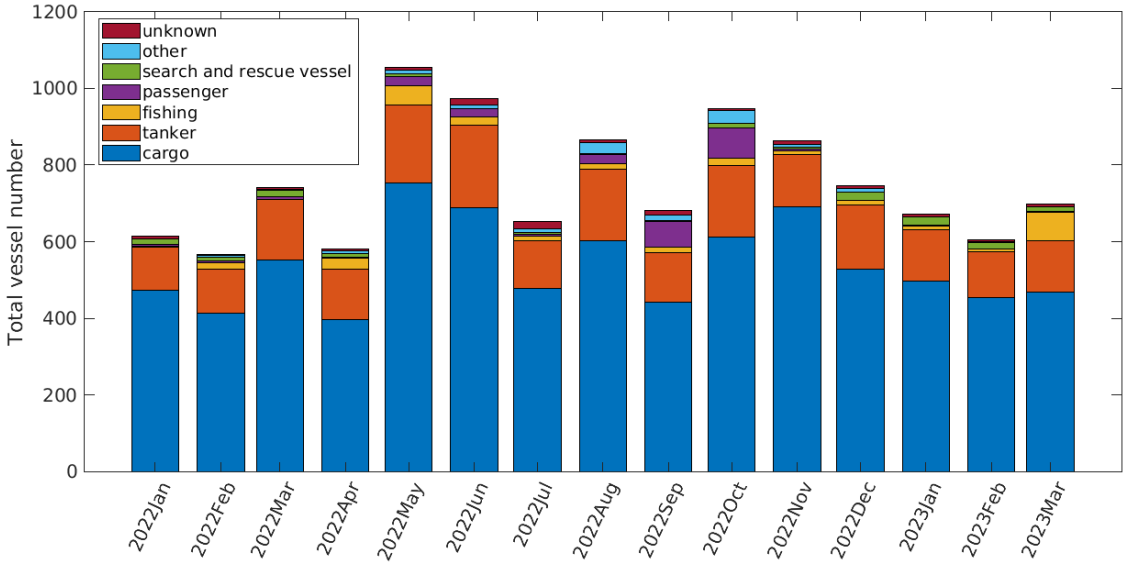

Figure 26. Monthly statistics of vessel types and numbers in the vicinity of the Cabot Strait moorings from January 2022 to March 2023.

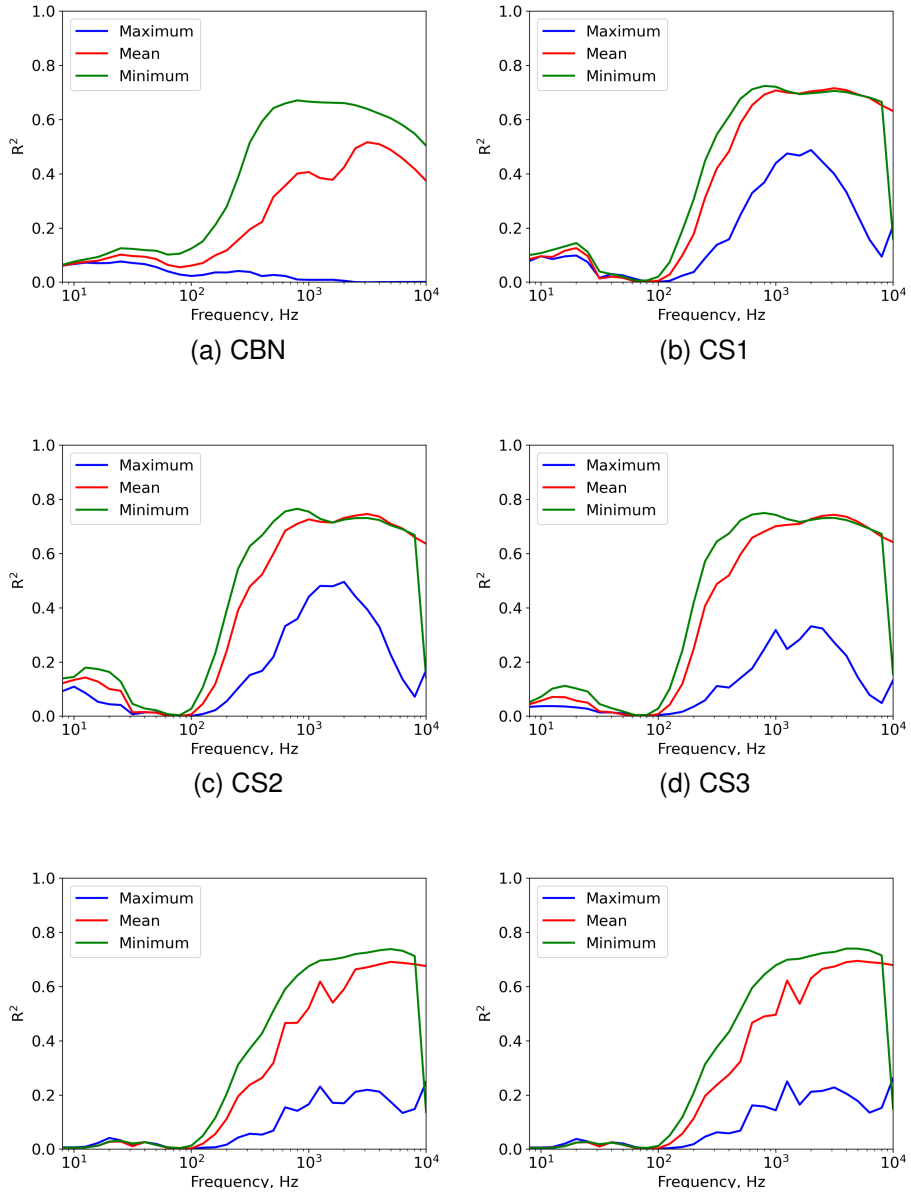

Figure 27. The correlation between wind speed and sound pressure level (hourly minimum, mean, and maximum) for different stations. Note that the sudden decrease around 8 kHz for CS1, CS2, CS3, and CSE is caused by low-pass filtering during the downsampling process.

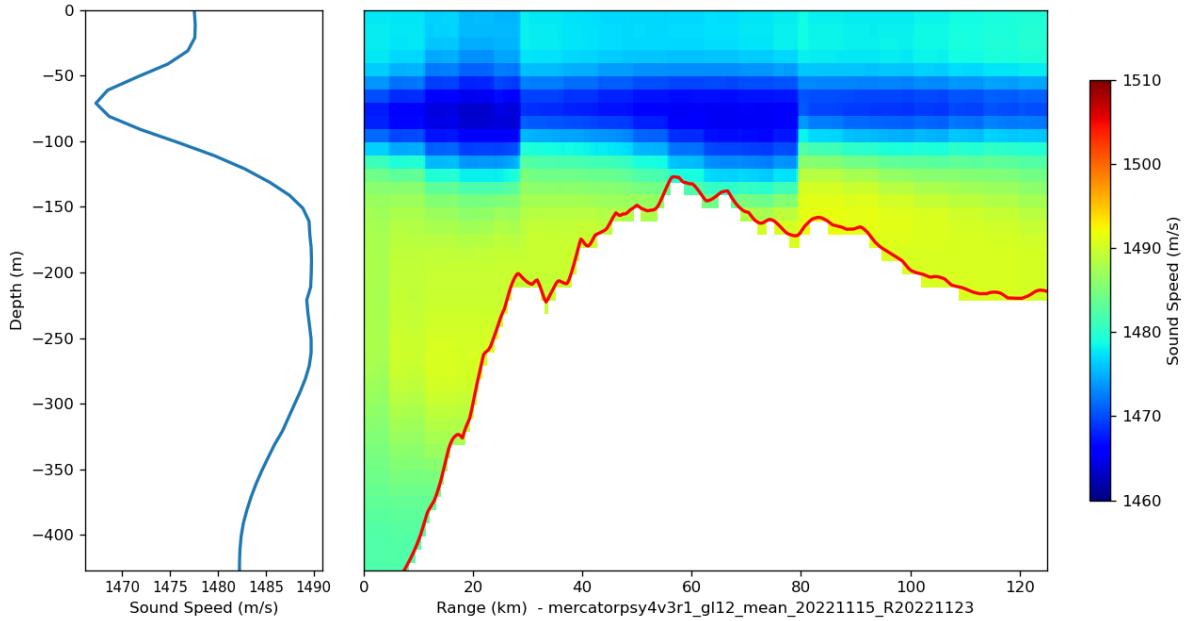

(a) Sound Speed for CS3: 100 degree W.R.T. due north

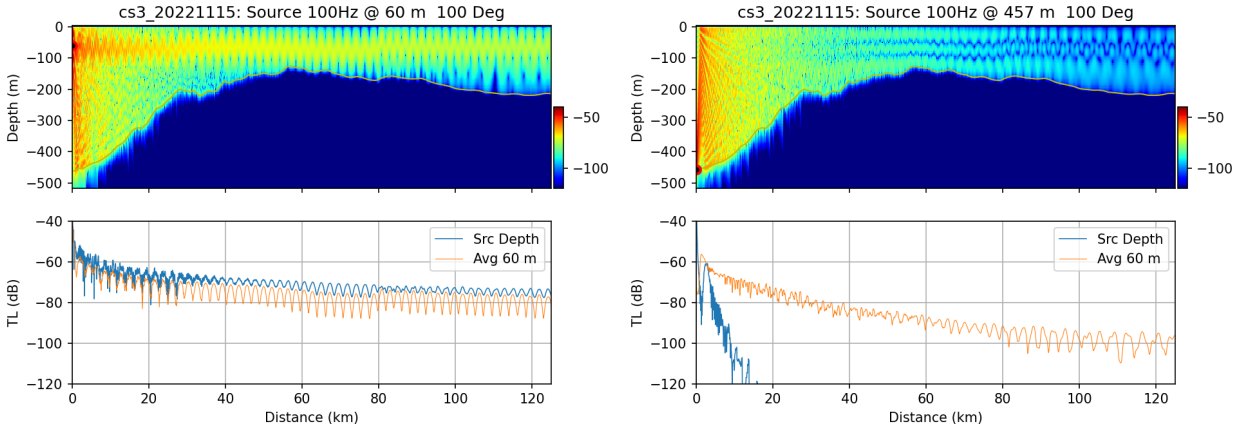

(b) Source depth at 60 m depth

(c) Source depth at 457 m depth

Figure 28. (a) Averaged sound speed profile and the range-dependent sound speed field for CS3 at an azimuthal direction of 100 degrees relative to due north. Panels (b) and (c) show sound propagation from a source at a depth of 60 m and 457 m, respectively, both with an azimuth of 100 degrees relative to due north in November 2022. The color scale in the upper sub-panels of (b) and (c) represent the transmission loss in dB.

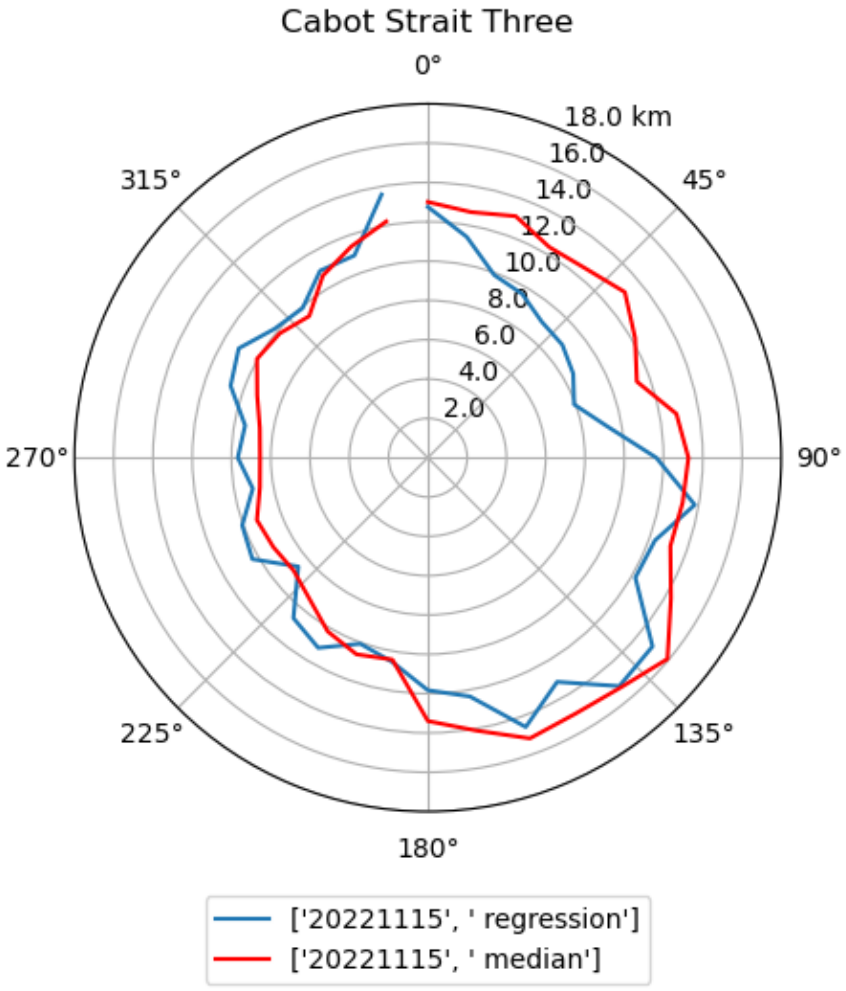

Figure 29. Monthly averaged detection range estimates for the CS3 station if the PAM system was at a depth of 60 m. The blue line shows results from the logarithmic regression model, while the red line shows estimates from the modified quantile regression model.